PERFORMANCE ANALYSIS OF SIMPLE-T AND 3D-HELICAL PASSIVE MICROMIXERS WITH NEWTONIAN AND NON-NEWTONIAN FLUID

A Thesis
Submitted in Partial Fulfilment of the Requirements for the Award of the Degree of

MASTER OF TECHNOLOGY
IN
THERMAL ENGINEERING

Submitted by:
SULEKH TOKAS
(2K18/THE/14)

Under the supervision of:
Dr. M. ZUNAID
(Asst. Professor)

DEPARTMENT OF MECHANICAL ENGINEERING
DELHI TECHNOLOGICAL UNIVERSITY
(Formerly Delhi College of Engineering)
Bawana Road, Delhi-110042, India.

JULY, 2020

CANDIDATE'S DECLARATION

I, **Sulekh Tokas** (Roll no: 2K18/THE/14) hereby declare that the Thesis entitled "**Performance Analysis of Simple-T and 3D-Helical Passive Micromixers with Newtonian and Non-Newtonian Fluid**" submitted in partial fulfilment of the requirement for the award of the degree of Master of Technology (M.Tech) in Thermal Engineering to the Department of Mechanical Engineering, Delhi Technological University (DTU), Delhi is an authentic work of my own carried out under the supervision of **Dr. M. Zunaid** (Assistant Professor) at Department of Mechanical Engineering, Delhi Technological University, Delhi, India. The current work has not been submitted to this or any other institution for the award of any degree, diploma, or fellowship or other similar titles of any sort.

The current thesis work has resulted in the publication of two research articles in peer-reviewed journals with details as follows:

(1.) Title of the Paper: **Numerical Investigation of 3D-Helical passive micromixer with Newtonian fluid and Non-Newtonian fluid Blood**.

Authors: Sulekh Tokas[1], Mohammad Zunaid[2], Mubashshir Ahmad Ansari[3]

Name of the Journal: Asia-Pacific Journal of Chemical Engineering (SCI-Expanded)

Status of the Paper: Accepted

Date of Paper Communication: 11/06/2020

Date of Paper Acceptance: 13/8/2020

Date of Paper Publication: NA

(2.) Title of the paper: **Computation Analysis of Passive Mixing in T-Micromixer with Non-Newtonian Blood**.

Authors: Sulekh Tokas[1] and Mohammad Zunaid[2]

Name of the Journal: International Journal of Mechanical and Production Engineering Research and Development (SCOPUS Indexed)

Status of the Paper: Published

Date of Paper Communication: 08/06/2020

Date of Paper Acceptance: 28/06/2020

Date of Paper Publication: 29/08/2020

SULEKH TOKAS
(2K18/THE/14)

SUPERVISOR CERTIFICATE

This is to certify that to the best of my knowledge, this thesis entitled **"Performance Analysis of Simple-T and 3D-Helical Passive Micromixers with Newtonian and Non-Newtonian Fluid"** submitted by Sulekh Tokas (2K18/THE/14) is his original work and has not been submitted for the award of any other degree in this or any other Institute/University.

I further certify that the information provided by the student on the number of publications and indexing is correct.

Place: Delhi

Date: 29.08.2020

Dr. M. Zunaid

Assistant Professor,

Department of Mechanical Engineering,

Delhi Technological University

(Formerly Delhi College of Engineering)

ACKNOWLEDGEMENT

I would like to take this opportunity to extend my deepest gratitude towards my supervisor **Dr. M. Zunaid**, Asst. Professor, Department of Mechanical Engineering for supporting this research and also for his consistent guidance, motivation throughout this journey. I consider myself to be fortunate to be a part of his team and work under his mentorship.

I would also like to thank my teachers and colleagues at Delhi Technological University for assisting me in the pursuit of this project.

Finally, I am greatly thankful to my family and friends for their non-stop support and motivation. This work would have not been possible without them.

Sulekh Tokas

(2K18/THE/14)

ABSTRACT

Mixing at micro-scales is purely governed by the diffusion mass transport phenomenon, which is a time-consuming process requiring a prolonged length of the microchannel to obtain desired results. The present study proposes a novel three-dimensional helical micromixer (TDHM) with a rectangular cross-section to achieve splendid mixing performance within a short distance contrary to the simple T-micromixer (STM). A thorough numerical investigation of mixing performance and fluid flow patterns have been conducted using the continuity, species transport, and the Navier-stokes equations with Newtonian and non-Newtonian fluid at a wide range of Reynolds number (0.2~320) and mass flow rate (0.00005 kg/hr~0.091 Kg/hr), respectively and a comparison between the results of STM and TDHM are presented.

Blood is selected as the Non-Newtonian fluid and its rheological characteristics are numerically captured by implementing the Carreau-Yasuda model, whereas water is used to study mixing with the Newtonian fluid. For the same mixing length of STM and TDHM i.e. 3000 microns it is found that at Re = 2, the mixing index of TDHM is 40. 5% more than that of the STM with water as the working fluid while for blood it is 34.3% and it is seen that TDHM performs better than the STM at all the mass loadings.

Once the results for the same mixing lengths are computed, another study is conducted fixing the axial lengths of STM and TDHM. Complete mixing (97.5%) is achieved for Newtonian fluid at Re=320 whereas the minimum efficiency observed is 74.3 % at Re = 66. Although for Non-Newtonian fluid (Blood) the conventional STM gives poor mixing with increased mass flow rate. However, TDHM furnish splendid mixing with 97% efficiency at the lowest mass flow rate of blood ($\dot{m}$) considered in the study, i.e. 0.00005 Kg/hr and 73.6 % at $\dot{m}$=0.091 Kg/hr. Therefore, it was concluded that the TDHM gives much better performance at much less axial distance than that of the STM at all values of the flow rates considered in the study making it an effective choice to be utilized for various biomedical, chemical, and biochemical applications.

TABLE OF CONTENTS

LIST OF FIGURES

LIST OF TABLES

NOMENCLATURE

L_a	The axial length of Simple T-mixer, µm
P_h	Pitch of the helical channel, µm
d_m	Mean diameter of the helical curve in TDHM, µm
L_m	Mixing or peripheral length of TDHM, µm
W_i	Width of the inlet channels, µm
W_0	Width of the outlet channel, µm
H	Height of the channel, µm
N	Number of turns in TDHM
L_e	Exit length, µm
ρ	Density of the fluid, Kg/m^3
x, y, z	Cartesian co-ordinates
u, v, z	Velocity components of the flow field in x, y, z directions, m/s
$\vec{V}$	Velocity vector, m/s
t	Time, seconds
b_i	Body force component, N
τ_{ij}	Stress Tensor, N/m^2
λ	Volumetric dilation coefficient
δ_{ij}	Kronecker delta
P	Pressure, KPa
D_{AB}	Coefficient of molecular diffusivity
C_A	Concentration of species
n	Power-law index

K	Consistency index
H	Apparent Viscosity of Non-Newtonian fluid, Pa-s
$\dot{\gamma}$	Rate of shear
η_0	Zero shear rate viscosity, Pa-s
η_∞	Infinite shear rate viscosity, Pa-s
λ	Characteristic relaxation time
D	Rate of deformation Tensor
Re	Reynolds Number
V_m	Mean Velocity of the flow, m/s
D_h	Hydraulic diameter of the microchannel, µm
Mi	Mixing index, %
σ^2	Actual variance in the mass fraction of the fluid component
σ_{max}^2	Maximum variance
c_i	Mass fraction at sampling point i
c_{avg}	Average mass fraction at a cross-section
ṁ	Mass flow rate of blood, Kg/hr

CHAPTER 1

INTRODUCTION

1.1 Microfluidics-An overview

The study of fluid flow at the microscale, i.e. the length scale of the systems being of the order of micrometres is termed as microfluidics. The concept of miniaturization of various chemical, biochemical, and biological analysis carries enormous advantages. First, there is a significant amount of reduction in the requirement of the sample size. For example, downscaling the linear scale by a factor of 10^4 will reduce the volume requirements by the order of $10^{12}$and such a lower volume of fluid helps in fast analysis and diagnosis. Second, shrinking down the actual size of chemical/ biological laboratories to the size of the chip will not only bring down the cost associated with set-up and running the laboratory by remarkable amounts but it also makes the laboratory compact and portable. The miniaturized version of an actual laboratory that performs functions such as mixing, pumping, separation, etc is known as Lab on a chip (LOC) device. These chips will also provide us with increased selectivity and sensitivity. Due to these advantages, Lab on a chip (LOC) technology has driven several critical research trends over the past few decades, particularly for applications in chemical and biological fields.

Although in microelectronics the behaviour of electrons remains almost the same even at the micro and nano scales, however, the scenario for fluids at the microscale is different with respect to the behaviour at macroscales. The physics of fluid flow changes drastically with length scales and one of the important dimensionless parameters characterizing the flow is the Reynolds number, Re. The flow at micro-scales is dominated by the viscous forces of the fluid contrary to the macro-scales where the inertial forces play a major role in flow dynamics. If we have to imagine swimming at a microscale, our motion will stop instantly due to the opposing viscous forces whereas in macroscales we observe the motion to continue for a longer period and distance due to the presence of inertia. Some applications of the microfluidics are discussed below:

1.1.1 Biomedical Diagnostics

One of the prominent applications of microfluidics is medical diagnosis. Currently, various microfluidic devices are being used for HIV diagnosis, pregnancy tests, screening of drug abuse, glucose biosensors, etc. This domain of microfluidics is termed as point-of-care (POC) which requires more exploration to produce several other devices that incur a low cost, are easy to use, and are portable making it feasible for a larger portion of population even living in the rural areas.

1.1.2 Analysis of biological macromolecules

To understand the properties and behavior of biological macromolecules like the DNA, RNA, proteins, etc, proper stranding and sequencing are needed. One such example is the DNA hybridization through microfluidics. It involves breaking the double-stranded DNA structure into a single-stranded DNA sequence for further analysis of a disease or infection. Figure 1.1 illustrates the basic building block of DNA structure known as nucleotide comprising of Nitrogenous base, sugar, and negatively charged phosphate group.

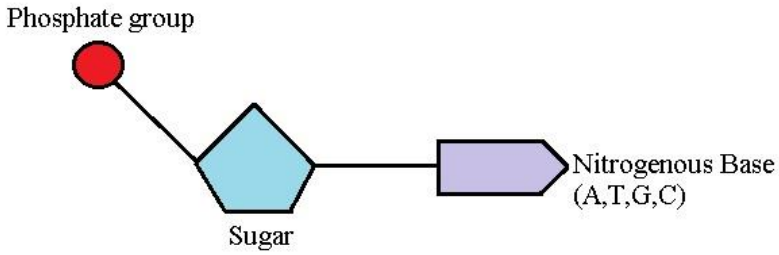

Figure 1.1 Basic DNA nucleotide

1.1.3 Drug delivery and blood extraction

The conventional methods of drug delivery and blood extraction involve using sharp syringes which are painful. Another drawback of using needles for drug delivery is the large time associated with the drug to be transported to the affected organ or area. However, employing microneedles is painless and can be directly used to deliver the drug close to the affected area reducing a significant amount of time due to the reduction in "drug path". Several microdevices are also available for testing blood sugar levels which

are very helpful for diabetic patients who need to keep track of their sugar levels on a daily basis.

1.1.4 Electronic cooling and Thermal management

With the reduction in the size of electronic components like microprocessors, Integrated circuits, etc. there comes a basic requirement of the effective dissipation of heat from these components to operate under the safe limit. Although the size of electronic components is getting smaller, however, the power input required to operate remains the same, and thus, removing the excess thermal energy from confined micro spaces is a challenge. Several droplets based microfluidic cooling systems and micro heat pipes have come out to be effective solutions to these problems. This domain is an extensive area of ongoing research and constant efforts are been made to construct optimal thermal designs in order to allow effective passive cooling for power components and modules.

1.1.5 Mixing and Reactive system analysis

Several chemical and biomedical applications like micro-chemical reactors, polymerization, organic synthesis demand rapid mixing of fluids to obtain homogenized samples and fast reactions between the fluids. The current thesis involves an investigation of passive micromixers and a detailed Section 1.2 covers the field of these micromixers discussing various types, working, and applications.

1.2 Micromixers

Micromixers are an essential part of various lab-on-chip (LOC) and micro total analysis systems (μTAS). In various microfluidic applications, the mixing efficiency of micromixers may affect the overall performance of the entire micro total analysis systems (μTAS). For example, fast mixing of cells, reagents, and organic solutions are essential in many bioengineering, biochemical systems, and nanomaterial synthesis. Efficient mixing not only improves the detection sensitivity but also brings down the analysis time by a notable factor. The physical phenomenon of mixing changes at microscales when compared to the mixing at macroscales. At macroscales, the mixing majorly depends on the convection mass transport which increases with the turbulent nature of fluid flow due to the rise in momentum transfer, however, the flow at microscale is highly streamlined

and laminar with no disordered random motion of the fluid. Hence, the mixing phenomenon is governed by molecular diffusion mass transport due to the dominance of viscous forces which demands the mixing fluids to stay in contact for a longer period of time and also requires long lengths of mixing channels. Since keeping the prolonged lengths of mixing channels rule out the basic idea and concept behind miniaturization of analysis systems, it is crucial to develop micromixers which are capable of giving effective mixing within a short period and lengths. Micromixers have numerous applications spread over a wide range of domains including:

- Polymerization
- Applications in crystallization
- Nuclear magnetic resonance (NMR) spectroscopy
- Organic synthesis
- The extraction process for chemical reactions
- Enzyme assay applications
- Biological Screening including both targeted cell sorting and selective sorting of biomolecules.
- Bio-analytical processes: cell separation, lysis, and DNA
- Protein folding

Based on the mechanism employed for mixing the fluids, micromixers can be broadly classified into categories namely, Active and passive micromixers.

1.2.1 Active micromixers

Active micromixers utilize external sources of energy like electrical field, magnetic field, vibrational energy, acoustic, rotational energy, pressure, etc as a stimulus to the mixing process in the microchannels [1]. These micromixers are complicated and require additional components which make it difficult to integrate into the micro-total analysis systems (μTAS). However, they give better control over the flow and the amount of mixing.

Electrical field-driven micromixers utilize the motion of electrically charged fluids in an electrical field (AC or DC) to disturb the interface of the mixing fluids which enhance the diffusion mass transport. This phenomenon is termed as the electro-hydrodynamic (EHD) instability [2]. Pressure field-driven micromixers are very common micromixers because of their simple construction and design. The basic design involves a simple T-channel with two micropumps to alternately inject the fluid into the mixing channel making it a pulsatile flow. Employing this type of arrangement greatly enhances the interfacial area resulting in improved mixing efficiency [3]. Some work has also been reported with

bubbles in a pressure field-driven micromixer. These bubbles when generated at a particular frequency will disturb the interface of the mixing fluids producing better mixing performance [4]. Micromixers driven by magnetic fields have magneto-fluids which are subjected to Lorentz forces with the help of magnets and electric fields. The magnetic field can serve both as a mixer and pump to drive the flow through the microchannel [5]. The electrodes are placed along the length of the conduit and the magnitude and direction of the magnetic field can be varied to control the flow dynamics of the electrolyte solution. Some designs also incorporate rotating magnets inside the channels to increase stirring action which will enhance the mixing efficiency [6]. A group of acoustically driven micromixers is based on bubble formation within the mixing channel to enhance the convective mixing. Some micromixers take advantage of the surface roughness of the walls of polydimethylsiloxane (PDMS) to form single or multiple bubbles. Another category of sound driven micromixer is which uses surface acoustic waves (SAW). The acoustic wave is made to pass the solid surface of the micromixer. The sound streaming increases the stirring effect which enhances the mixing index. Figure 1.2 illustrates and summarizes the classification of active micromixers.

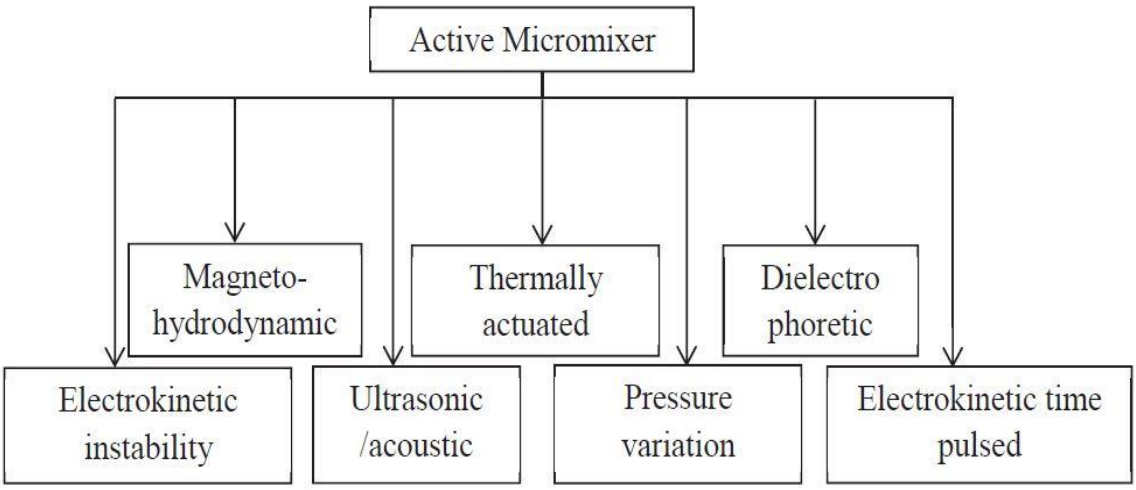

Figure 1.2 Types of Active Micromixer

Additionally, some micromixers also use the centrifugal forces imparted due to rotation to achieve good mixing. For example, Lab on CD micro-total analysis system has various components mounted on a disc which is rotated about an axis to evenly mix the fluids. The Coriolis effect comes into the picture due to the rotation and thus the mixing is

strongly dependent on this component of force. The rotation per minute (rpm) of the disc can be varied to control the amount of mixing needed according to the requirements [7].

1.2.2 Passive micromixers

As mentioned above, active micromixers utilize external energy sources to enhance the mass diffusion process. However, passive micromixer also known as the static micromixer is different in the sense that it uses modification in geometry, shape, and size of the mixing channel to form vortices, produce chaotic advection, etc. The basic concept behind passive micromixer is to stretch and fold the flowing fluid number of times which magnifies the interfacial area of the mixing fluids increasing diffusion mass transport within a short distance and time. The major advantage of a passive micromixer is that it is simple to construct and integrate into a system and thus, the cost of running and manufacturing is very less making it an attractive mixer for exploration and several types of micromixers are developed by various scientists and researchers. Figure 1.3 depicts the types of passive micromixers. Since the current work of the thesis is based on passive micromixers, detailed background information and literature review are provided in chapter 2.

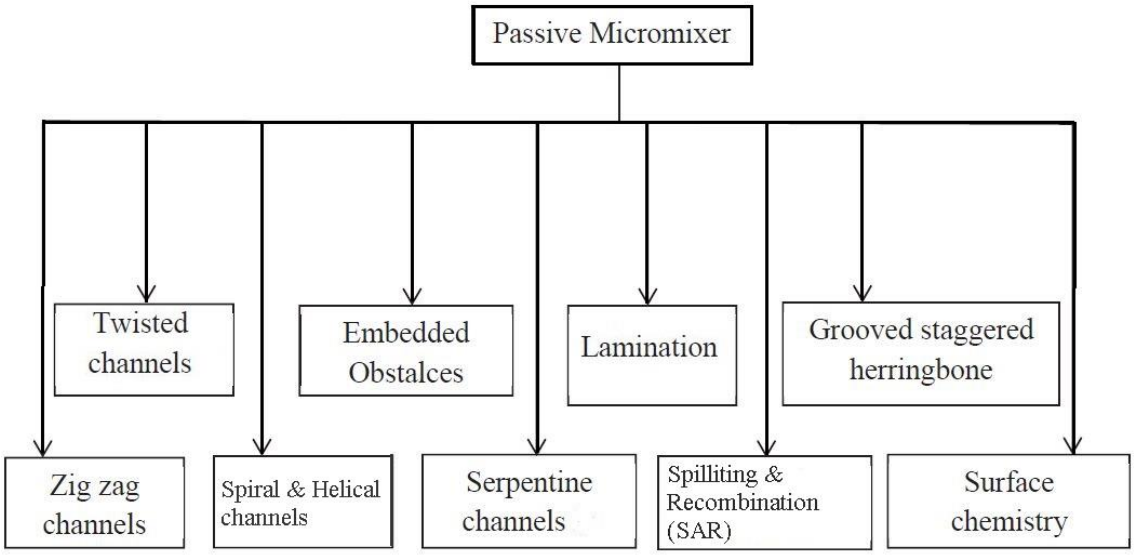

Figure 1.3 Classification of passive micromixers

1.3 Objectives of the Thesis

The thesis work investigates the mixing performance of both Newtonian fluid & Non-Newtonian fluid blood in various effective passive micromixers and presents a deep study of the flow behavior of the fluids inside the microchannels. Computer-aided design (CAD) modeling is executed using the available commercial software Solidworks whereas the numerical simulations were performed to solve the continuity, Navier-Stokes equation, and species transport equation of mass transport using the CFD solver in the software Ansys Fluent. The specific objectives of the thesis can be summarised as:

i. To evaluate the mixing efficiency of the three-dimensional helical passive micromixer (TDHM) and the conventional T-micromixer (STM) for a wide range of flow rates and Reynolds number, Re.
ii. Investigate the rheological flow characteristics of blood in microchannels and how does it differ from the flow behaviour of Newtonian fluid (Water in current work).
iii. To study the pressure drop between the inlet & the outlet of the micromixers to examine the energy requirements.

1.4 Thesis Outline

The current thesis consists of 5 chapters in total. The first chapter forms the basis of the work providing an introduction to the domain of microfluidics and micromixers. The second chapter consists of an in-depth discussion on the type of micromixers and the existing literature involving both experimental and numerical work. Chapter 3 discusses the governing partial differential equations used for the numerical solutions, a study on the grid sensitivity, behaviour of Newtonian and Non-Newtonian fluids, Validations of the computational approach with the existing literature, and numerical solution methodology implied in the study. Chapter 5 consists of the numerical solution obtained for STM and TDHM with both Newtonian (water) and Non-Newtonian fluid (Blood) as the working fluid in the micromixers. Finally, chapter 5 provides a brief conclusion of the work and the scope of the future in the field.

CHAPTER 2

LITERATURE REVIEW

Microfluidics is an interdisciplinary domain of applied science which deals with exploring the flows with a characteristic length of the order of microns. It has widespread applications in various biomedical diagnostics, mixing & reactive system analysis in chemical engineering, biochemical domains, electronic cooling, and micro-technology for thermal management [8]. The miniaturized version of an actual laboratory that performs functions such as mixing, pumping, separation, etc is known as Lab on a chip (LOC) device, giving several advantages like low volume to the surface ratio for enhanced heat transfer and small inventory requirements. The basic drawback of biological and chemical microprocessing is the inefficient mixing due to the absence of the turbulence and the entire flow being laminar in nature. In this case, the mixing process entirely depends on the molecular diffusion phenomenon which is a very slow process and may require a prolonged length of the microchannel to obtain the desired results, thus enhancement of mixing in microchannels has attracted numerous research work which can be studied in the extensive review literature [1], [9], [10]. Micromixers are broadly classified into two wide categories as active and passive micromixers. Active micromixers make use of external energy sources such as electric force, magnetic force, acoustic wave, etc to control and drive the mixing process inside the microchannels and hence are difficult & costly to integrate into the device. Whereas passive micromixers utilize the variation of the geometrical shape of channels to advance the mixing results, therefore they are easy to fabricate, operate, and are more cost effective [11], [12]. Since the current study is based on passive micromixers, the literature review covered in this chapter is restricted to the currently available work on passive micromixers.

2.1 Basic T-micromixer

The basic micromixer is the T-junction type mixer and extensive work has been reported describing the three types of flow regimes in this type of micromixer. Several early work in the field of micromixers involved the fabrication of microchannels using silicon. Koch et al. [13] compared two basic micromixers and characterized the mixing using the ammonia in water solution and phenolphthalein solution. Veenstra et al. [14] proposed a novel silicon-based micromixer which produced effective mixing of water and phenolic

solution. Gobby et al. [15] studied the mixing pattern in a simple T-mixer for non-reactive gases possessing different viscosities using CFD simulations. The effect of various operating and design parameters like aspect ratio (height/width ratio of the main mixing channel), inlet flow rates, angle of the inlet channels, etc was studied. It was found that at low flow rates, the mixing length required is less. Also, more accurate results were obtained in 3-dimensional simulation as compared to the results in a 2-dimensional study. Bothe et al. [16] studied the heat transfer and mixing performance in T-microreactor. It was concluded that reactions at the micro-scale provide better thermal control and chemical reactions take place at a faster rate. They also used CFD simulations to understand the three types of flow regimes seen in the T-micromixer and found that engulfment zone flow provided higher mixing. Wong et al. [17] investigated the mixing performance of T-micromixer experimentally and numerical simulations were used to get an insight into the flow characteristic within the microchannel. Micro T-mixer was fabricated using the silicon substrate which was attached on a Pyrex glass plate. It was found that a pressure of 5.5 bar at inlets was sufficient to mix the two fluids completely within a fraction of a second for a microchannel having a hydraulic diameter of 67 μm. Soleymani et al. [18] utilized CFD to study the flow and mixing characteristics and proposed optimized results for effective mixing in the liquid phase. It was concluded that secondary flow and vortices are important for obtaining excellent qualitative mixing. Depending on the value of Reynolds number for flow through the main microchannel, the flow was characterized in three different regimes, namely stratified flow, vortex flow, and engulfment flow. A significant rise in the mixing performance was witnessed at higher Reynolds number (Re $\geq$130) due to the flow entering the engulfment regime where asymmetrical path lines were observed and finally, an optimized TT-mixer was presented for effective mixing in the liquid phase. Andreussi et al. [19] performed an in-depth examination of the flow regimes in a simple-T micromixer using direct numerical simulations (DNS) which are considered to be a method of great accuracy. The flow patterns were investigated on channels with three different aspect ratios (width to height ratio of the main mixing channel), i.e. 0.75, 1 & 2. The mixer with aspect ratio 2 showed different evolvement of flow as compared to the other two. As the Reynolds number increased, the flow shifted from vortical to asymmetric and then finally to chaotic at very high Reynolds number. Matsunaga et al. [20] proposed a novel low-cost simulation technique based on particle tracking to obtain mixing behaviour in T-micromixer with a rectangular cross-sectional area having high Schmidt number=3600. The results obtained

from this model were compared with the results obtained from the backward random walk Monte Carlo simulations. The results were in good agreement. Moreover, it was found that ordinary grid-based simulations did not predict accurate mixing performance at high Reynolds numbers, especially in the engulfment flow regime of the micromixer. Ansari et al. [21] investigated the effect of the position of interfaces of fluid streams on the mixing performance including both single and double faces of the fluid streams for low Reynolds number range (0.1~10). It was found that the effect of position of interface is more significant for Reynolds number below 10 due to the fact that the mixing phenomenon is highly dominated by the molecular diffusion mass transport, whereas at higher values of Reynolds number (Re>10), the effect of position of interface on mixing diminishes. Lobasov et al. [22] numerically performed a study on a wide range of height and width of the mixing channel of the simple T-micromixer. Furthermore, the correlations for calculating the critical Reynolds number and the pressure drop were presented having good accuracy.

2.2 Modifications in Simple T-micromixer

Several geometrical modifications were suggested in the micro T-mixer to enhance the mixing performance of the device. Cortes-Quiroz et al. [23] proposed a three-dimensional structure by placing the inlets of simple T-mixer at different horizontal levels which resulted in enhanced mixing of the streams. Sarkar et al. [24] studied the effects of different wall protrusions with the help of numerical simulations and the results were compared with that of the basic T-mixer. Dundi et al. [25] imparted swirls at inlets to induce dean vortices and numerical results showed better results of mixing efficiency at both low and high Reynolds numbers. Lobasov & Minakov [22] numerically examined the effect of various parameters in a micro T-mixer namely, density, viscosity, rheological behaviour, inlet temperature difference of the two fluids, and also the effect of gravity on the mixing process. The results for mixing the index were plotted and compared for each parameter. Bhagat et al. [26] utilised the obstruction of different shapes namely, diamond, circular, triangular, and stepped diamond in the main mixing channel of the micromixer to enhance the mass transport due to the splitting and recombination of mixing streams. CFD simulations were carried out to investigate the performance of different obstructions and also to optimize the micromixer. Since the modification involved making a few simple changes, it is easier to integrate these mixers on to the lab-on-chip devices.

Moreover, a very less pressure drop of 150 Pa was recorded for 11mm mixing length reducing the pumping power requirements. Mouheb et al. [27] investigated the performance of a cross-shaped micromixer both numerically and experimentally and compared the results with that of the simple T-micromixer. A cross-shaped micromixer showed significant improvements in the mixing between the two fluids considered in the study due to the vortex stretching and enhancement in the shear rate. Also, the pressure drop was far less in the cross-shaped micromixer giving it an added advantage of low pumping power requirements. Kashid et al. [28] evaluated the mixing characteristics in five different generic micromixers namely, T-square, T-trapezoidal, Y-rectangular, Concentric, and caterpillar micromixers using the method which is based on the Villermaux–Dushman reaction. It was found that out of the five micromixers considered in the study, caterpillar micromixer performed the best at both low and high Reynolds number with lower mixing time. Hossain & Kim [29] modified the simple micro channel of T-mixer with straight grooves and investigated the effect of various geometrical parameters on the mixing performance of the mixer. Three arrangements of patterned walls are studied that are, single wall with patterns, both the walls having symmetrical patterns and finally both the walls having asymmetrical patterns. It was seen that with an increase of grooves per cycle (ranging from 8 to 20), the mixing index increased contrary to the pressure drop which reduced with an increase of grooves. The mixer with both walls having asymmetrical patterns performed better than the other two mixers. Sarkar et al. [30] studied various novel types of microfluidic junctions named as 1-1 and 1-2 type of micro junctions with the help of CFD simulations and a comparison is presented for the mixing performance. It was found that 1-2 micromixers performed better than 1-1 junction micromixers and 1-2 junction mixer given the name OA 100–200–1650 WY-junction provided splendid mixing out of all the mixers considered in the study.

2.3 Curved and helical Micromixers

Another way to increase the mixing process is to increase the interfacial area between the mixing fluids by using curved and helical channels which also imparts swirling strength to the flow resulting in enhancement of the diffusion process. Hossain et al. [31] numerically evaluated the mixing process between water and ethanol in three different micromixers consisting of curve channel, square-wave channel, and zig-zag channel. Though the performance of each micromixer was almost the same at low Reynolds

number (1~15), however, the square-wave channel showed the best result out of the three at higher Reynolds number due to the strong secondary flow. Afzal & Kim [32] came up with a novel passive micromixer with wavy walls of sinusoidal pattern and found that the shorter wavelength mixers developed stronger secondary flows and thus better mixing was achieved even at low Reynolds numbers as compared to the longer wavelength sinusoidal micromixers. Rampalli et al [33] replaced the earlier available square-wave channel of micromixer with the convergent-divergent micro-channel and numerically studied the performance and flow patterns of the square wave convergent-divergent micromixer (SQW-CD). They found that the mixing performance improved for high Reynolds number ($Re>10$), however, there was not much significant difference in the mixing index at low Reynolds number ($Re<10$). Balasubramaniam et al. [34] experimentally and numerically examined the mixing behaviour of Newtonian fluids for an in-plane spiral shape mixer with different cross-sectional geometries namely, square, semi-circular, rectangular, and trapezoidal. Employing semi-circular and trapezoidal cross-sections showed notable improvement in the mixing index without much change in the pressure drop of the micromixer. Rafeie et al. [35] proposed a novel fine-threaded lemniscate-shaped micromixer design. Numerical and experimental studies showed that for very small Reynolds number flow ($Re\leq1$), 100 percent mixing was achieved in both straight channel and proposed designs, a sharp drop was witnessed in mixing efficiency of a straight channel mixer as the Reynolds number exceeded the value of 1, however, the mixing index of the proposed design was reported above 90 percent at all the mass flow rates. Yang et al. [36] presented a new 3-dimensional micromixer design consisting of two layers of spiral channels connected with a vertical erect channel. Several experimental research works are available for the 3-dimensional helical micromixers with circular channels. Liu et al. [37] experimentally examined the mixing performance of a three-dimensional helical micromixer having a circular cross-section. The complex design was fabricated in fused silica using FLICE and laser technology. The mixing length required in this case was compared to the mixing length of the straight channel and it was seen that superior mixing was achieved at far lesser length in the case of three-dimensional helical micromixer fulfilling the need for compactness of overall micro-system serving as the basic purpose of miniaturization. Tachibana et al. [38] used micro-lost wax casting to fabricate the three-dimensional helical micromixer. The molds for the casting process were prepared using the 3D-printing technology with hard wax resin as the construction material. Additionally, CFD studies were conducted to find the optimum

design of the micromixer, and 80% mixing was achieved at just 2mm axial distance having a 0.5mm distance between two adjacent grooves of helix structure. Shan et al. [39] fabricated two different types of effective 3-dimensional helical micromixer having three inlets and single outlet using femtosecond laser wet etch technology. Experiments were performed to examine the mixing characteristics with NaOH solution entering from inlet and phenolphthalein solution from the other two corresponding to a low Reynolds number of 2.6. Complete mixing (> 90%) was observed at a short length of 400 μm which just after the third turn of the helix. Finally, it was concluded that helical micromixers are highly effective to get complete mixing within a very short span of length.

2.4 Micromixers with Non-Newtonian fluids

Several applications in the field of biomedical and chemical demand to mix fluids exhibiting Non-Newtonian characteristics including both shear thinning and shear thickening rheological properties. Thus, various numerical and experimental work has been conducted by researchers considering the rheological effects. Islami et al.[40] numerically investigated the performance of various curved micromixers with Non-Newtonian power-law fluids. A decreasing pattern of mixing index was observed between Reynolds numbers 0.1 and 5, whereas the mixing performance increased significantly thereafter. Islami and Khezerloo [41] performed CFD simulations to examine the effect of grooves and its geometrical parameters on the performance of a curved microchannel for both Newtonian and Non-Newtonian fluids. Additionally, Non-Newtonian fluids with different power-law indices were studied and they found that at a fixed Reynolds number, mixing index increases with an increase of power-law index value. Carrier et al. [42] conducted experiments to examine the pressure drop in a caterpillar micromixer (CPMM) for Newtonian and several Non-Newtonian fluids. The results depicted that for Newtonian fluids, the friction factor scaling was related to f/2=24/Re. Also, viscoelastic fluids showed a higher pressure drop for all the static mixers. Afzal & Kim [43] used the carreau-Yasuda and Casson model to approximate the rheology effects of blood flow in a straight (T-junction) and a serpentine micromixer. Serpentine micromixer displayed better mixing results for all the wide range of mass flow rates that were considered in the study. Husain et al. [44] performed numerical simulations for blood and water using various models available for blood flow namely, the Carreau-Yasuda model, Casson model, power-law model, and Herschel Bulkley model in a serpentine micromixer based

on splitting and recombination of mixing streams with offset inlets. The results obtained from the proposed micromixer were compared with the results of several existing micromixers. It was found that mixing performance of the novel micromixer was close to the performance of the 3D serpentine micromixer and at a high number of mixing units, all the micromixers approached almost the same value of mixing index. Kuo et al. [45] experimentally and numerically investigated performance plasma mixing in three types of micromixers that is square-wave, zig-zag, and curved micromixers completely driven by the capillary action. The square-wave micromixer performed better out of the three due to the presence of stronger secondary flow giving 76% mixing efficiency in 4 seconds. Moreover, the square-wave mixer was picked for optimization and four different square-wave mixers were examined to predict the best dimensions of the square-wave. In addition, Vast literature is available discussing the flow dynamics and mixing process for Non-Newtonian blood [46]–[49].

2.5 Concluding Remarks

It is clear from the brief literature review that although widespread work exists for numerous micromixers with Newtonian fluids, yet limited work is available for Non-Newtonian fluids specifically blood. Since most of the biomedical and biochemical applications involve non-Newtonian fluids, therefore examining the behaviour of blood at microscale becomes important. In the present study, the mixing performance of two types of micromixers namely the conventional T-micromixer (STM) with a straight channel and a novel three-dimensional helical micromixer (TDHM) with a rectangular cross-sectional area was studied. Carreau-Yasuda model [32], [44] was used to capture the Non-Newtonian behaviour of viscosity of blood, whereas water was used as the Newtonian fluid. A comparative study of flow dynamics and mixing index between the Newtonian and the Non-Newtonian fluid is addressed for both the micromixers with the help computational fluid dynamics (CFD) simulations

CHAPTER 3

METHODOLOGY AND MODELING DETAILS

The numerical methodology to investigate the passive mixing include the development of flow domain, mesh generation, employing CFD-solver to iteratively solve the discretized governing equations, and finally, CFD-post processing to visualize the flow and mass transport between the fluids. Chapter 3 discusses the necessary governing partial differential equations that are continuity, the Navier-stokes equation, and the species transport equation to capture the molecular diffusion during the mixing. Since the current study involve examining the behaviour of both Newtonian fluid water and Non-Newtonian fluid blood, the appropriate model used to capture the rheological behaviour of blood is explained in detail and the relevant modifications in the governing partial differential equations due to the Non-Newtonian behaviour of blood is considered. The crucial boundary conditions and schemes used in the CFD solver are also discussed in detail in section 3.4. Section 3.6 elaborates on the mesh generation phenomenon and grid sensitivity analysis, i.e. comparing the results concerning the size of the grid used in the flow domain. Finally, in section 3.7, the validation of the computational method employed in this thesis is presented. The results for both Newtonian and Non-Newtonian were compared with the work accomplished in the existing literature.

3.1 Model and domain description

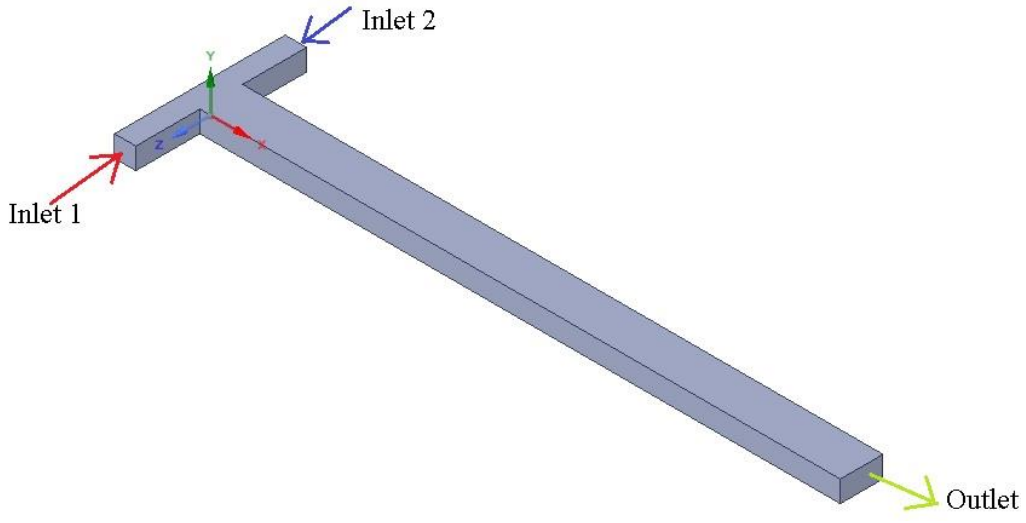

Figure 3.1 A Simple T-micromixer

Two micromixers are selected for the analysis. The simple T-mixer (STM) with a straight channel and three-dimensional helical micromixer (TDHM) with a rectangular cross-section as shown in Figures 3.1 and 3.2 respectively. The inlet channels of both the micromixers have 100 µm × 100 µm square cross-section whereas the outlet has a rectangular cross-section of 200 µm × 100 µm dimension. The aspect ratio which is defined as the width to height ratio of the microchannel is 2 for the main mixing channel and 1 for the inlet channels. The axial length of the simple T-mixer is fixed at L_a=3000 µm(3mm). All the parameters used to define the TDHM is depicted in figure 3.3. The dimensions of pitch (P_h) and mean diameter (d_m) of the helix curve is 0.370 mm and 0.38 mm respectively. All the geometrical parameters of TDHM are summarised in Table 3.1. The mixing length or the peripheral length of the helical channel can be calculated by the following relation

$$L_m = N\left[\sqrt{(\pi d_m)^2 + P_h}\right] \tag{3.1}$$

Where N denotes the number of turns in the helical curve.

Table 3.1 Geometrical Parameters chosen to define the TDHM

Geometrical Parameter	**Value**
Width of inlet channels (W_i)	100 µm
Width of the outlet channel(W_0)	200 µm
Height of the channel (H)	100 µm
Aspect Ratio of the mixing channel (A*)	0.5
Mean diameter of the helical curve (d_m)	380 µm
Pitch of the helical curve (P_h)	370 µm
Number of turns	7
Peripheral Length of the helical curve (L_m)	8.75 mm
The axial length of the helical curve (L_a)	3000 µm
Exit length (L_e)	150 µm

To perform a comparative study, two different comparisons were studied. First, the mixing evaluation is done when the axial length of TDHM is taken to be equal to the axial length of the STM, i.e. 3000 µm. Another study was also conducted on TDHM having the same mixing length or the peripheral length equal to the mixing length of 3000 µm which corresponds to an axial length (L_a) of 0.741 mm. It is to be noted that for a simple straight channel as in the case of STM, the axial length and the mixing length are equal. Also, the Reynolds number and mass flow rate used in the study are based on the velocity and hydraulic diameter of the main channel of the micromixer calculated on the dimensions of the main mixing channel, i.e. 200 µm × 100 µm.

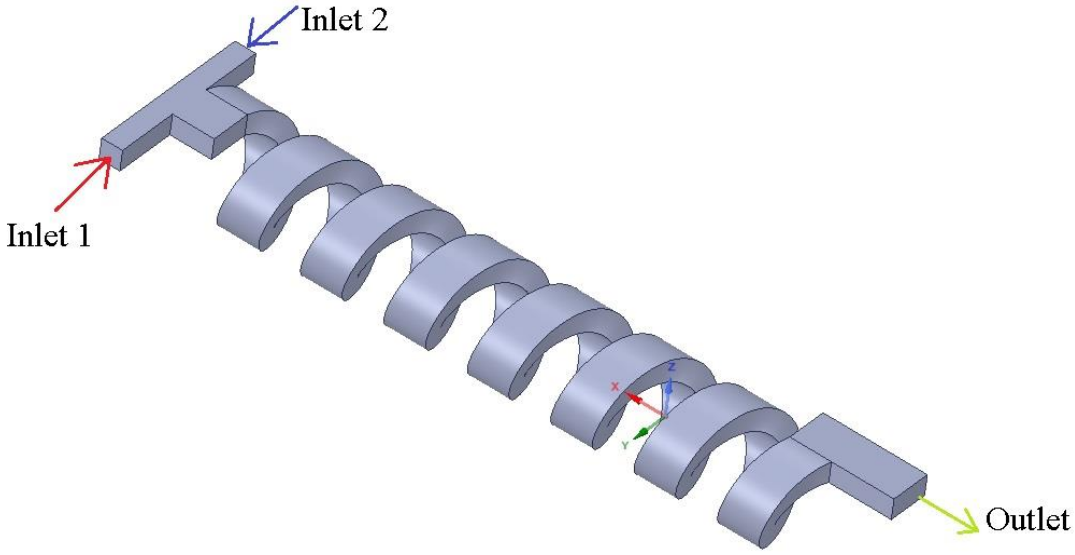

Figure 3.2 3-Dimensional Helical Micromixer (TDHM)

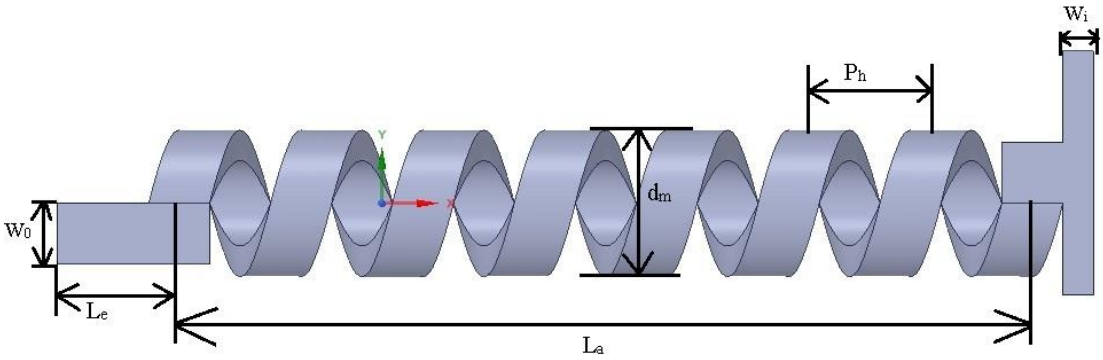

Figure 3.3 Parameters chosen to define the TDHM

3.2 Governing equations

3.2.1 The continuity equation

The continuity equation represents the phenomenon of mass conservation. The general equation of continuity in differential form cartesian coordinates is given as

$$\frac{\partial(\rho)}{\partial t}+\frac{\partial(\rho u)}{\partial x}+\frac{\partial(\rho v)}{\partial y}+\frac{\partial(\rho w)}{\partial z}=0 \tag{3.1}$$

Where ρ is the density of the fluid. u, v, w represents the velocity components of the flow field in x, y, z directions respectively and t is the time. Although equation 3.1 represents the general form, the equation simplifies due to several assumptions including steady and incompressible flow in the case of Newtonian fluids.

$$\frac{\partial u}{\partial x}+\frac{\partial v}{\partial y}+\frac{\partial w}{\partial z}=0 \tag{3.2}$$

The equation can also be written in an alternative form using the del operator representing the divergence of the velocity vector is given by equation 3.3.

$$\nabla.\vec{V}=0 \tag{3.3}$$

Where, $\vec{V}$ is the velocity vector and ∇ is the del operator

$$\nabla=\frac{\partial}{\partial x}\hat{\imath}+\frac{\partial}{\partial y}\hat{\jmath}+\frac{\partial}{\partial z}\hat{k} \tag{3.4}$$

$$\vec{V}=u\hat{\imath}+v\hat{\jmath}+w\hat{k} \tag{3.5}$$

The dot product of del operator and velocity is known as the divergence of the velocity field.

3.2.2 Navier-stokes equations

The Navier-stokes equations are considered to be the fundamental equation of fluid dynamics as it is derived from the basic law of conservation of momentum. This equation consist of the body force terms that act on a differential fluid element when it is placed in

a gravitational field, electrical field, magnetic field, etc or combination of these and the surface forces including both normal & shear stresses arising due to the pressure and viscid behavior of the fluid, respectively. The most generalised form of the momentum equation is as follows written with the index notation.

$$\frac{\partial(\rho u_i)}{\partial t} + \frac{\partial(u_i u_j)}{\partial x_j} = \frac{\partial(\tau_{ij})}{\partial x_j} + b_i \tag{3.6}$$

The right hand of the equation represents the sum of all the forces acting on the fluid element. Where, b_i is the body forces i.e. the force which is acting on every single particle of the fluid, τ_{ij} is the stress tensor given by:

$$\tau_{ij} = -p\delta_{ij} + \lambda \frac{\partial u_k}{\partial x_k}\delta_{ij} + \mu\left[\frac{\partial u_i}{\partial x_j} + \frac{\partial u_j}{\partial x_i}\right] \tag{3.7}$$

Where δ_{ij} is Kronecker delta, whose value is 1 when i=j and zero (0) for i≠j. λ is the volumetric dilation coefficient, μ is the coefficient of dynamic viscosity and $\frac{\partial u_k}{\partial x_k}$ signifies the volumetric deformation, whereas $\left[\frac{\partial u_i}{\partial x_j} + \frac{\partial u_j}{\partial x_i}\right]$ is the deformation caused due to shear stresses which act on the fluid element.

Since the fluid flow in the present work is assumed to be steady incompressible flow, the force due to the gravitational field is neglected and implying the stokes hypothesis, the equation 3.6 can be written for x, y and z-direction respectively as

$$\rho\left(u\frac{\partial u}{\partial x} + v\frac{\partial u}{\partial y} + w\frac{\partial u}{\partial z}\right) = -\frac{\partial p}{\partial x} + \frac{\partial \tau_{xx}}{\partial x} + \frac{\partial \tau_{yx}}{\partial y} + \frac{\partial \tau_{zx}}{\partial z} \tag{3.8}$$

$$\rho\left(u\frac{\partial v}{\partial x} + v\frac{\partial v}{\partial y} + w\frac{\partial v}{\partial z}\right) = -\frac{\partial p}{\partial y} + \frac{\partial \tau_{xy}}{\partial x} + \frac{\partial \tau_{yy}}{\partial y} + \frac{\partial \tau_{zy}}{\partial z} \tag{3.9}$$

$$\rho\left(u\frac{\partial w}{\partial x} + v\frac{\partial w}{\partial y} + w\frac{\partial w}{\partial z}\right) = -\frac{\partial p}{\partial z} + \frac{\partial \tau_{xz}}{\partial x} + \frac{\partial \tau_{yz}}{\partial y} + \frac{\partial \tau_{zz}}{\partial z} \tag{3.10}$$

The Navier-Stokes equation utilizes the divergence of the stress tensor, $\nabla.\tau$, The stress tensor can be represented in the form of a 3X3 matrix as

$$\tau = \begin{bmatrix} \tau_{xx} & \tau_{xy} & \tau_{xz} \\ \tau_{yx} & \tau_{yy} & \tau_{yz} \\ \tau_{zx} & \tau_{zy} & \tau_{zz} \end{bmatrix} = \begin{bmatrix} -p + 2\mu\dfrac{\partial u}{\partial x} & \mu\left(\dfrac{\partial v}{\partial x} + \dfrac{\partial u}{\partial y}\right) & \mu\left(\dfrac{\partial w}{\partial x} + \dfrac{\partial u}{\partial z}\right) \\ \mu\left(\dfrac{\partial v}{\partial x} + \dfrac{\partial u}{\partial y}\right) & -p + 2\mu\dfrac{\partial v}{\partial y} & \mu\left(\dfrac{\partial w}{\partial y} + \dfrac{\partial v}{\partial z}\right) \\ \mu\left(\dfrac{\partial w}{\partial x} + \dfrac{\partial u}{\partial z}\right) & \mu\left(\dfrac{\partial w}{\partial y} + \dfrac{\partial v}{\partial z}\right) & -p + 2\mu\dfrac{\partial w}{\partial z} \end{bmatrix} \quad (3.11)$$

The viscosity, μ is a property of the fluid. It can be a constant as in the case Newtonian fluids, however, it may vary with the temperature, time, and the shear strain rate. These types of fluids fall under the category of Non-Newtonian fluids. Section 3.3 briefly discusses both Newtonian and Non-Newtonian fluids and also introduces the Carreau-Yasuda model which is employed to numerically capture the rheological behaviour of the Non-Newtonian Blood studied in the thesis.

3.2.3 The species transport equation

The flow at the microscale is purely laminar, therefore the only possible way by which mixing can occur between two fluids is through the diffusion of molecules from one fluid to the other once they come into the direct contact. To visualize and quantify the mixing phenomenon, the equation of conservation of species need to be solved in the flow domain with correct boundary conditions. The species transport equation of advection-diffusion type in the for a steady-state flow is given as follows.

$$\left(\vec{V}.\nabla\right)C_A = D_{AB}\left[\frac{\partial^2 C_A}{\partial x^2} + \frac{\partial^2 C_A}{\partial y^2} + \frac{\partial^2 C_A}{\partial z^2}\right] \quad (3.12)$$

Where, $\vec{V}$ is the velocity vector, C_A is the concentration of species A and D_{AB} is the coefficient of molecular diffusivity.

3.3 Newtonian and Non-Newtonian fluids

According to Newton's law of viscosity, at constant temperature and pressure, the simple shear stress (τ) is proportional to the shear rate ($\dot{\gamma}$) and the constant of proportionality is commonly known as the dynamic viscosity (μ). It infers that the shear stress increases linearly with an increase in the shear rate. The fluids which demonstrate this type of behaviour are called Newtonian fluids. Most of the fluids which possess low molecular weight such as various organic and inorganic liquids, molten metals, water, and a wide

variety of salt solutions exhibit Newtonian behaviour when acted upon by the shear stress causing the fluid flow. It is observed that with an increase in either temperature or pressure, the viscosity of gases tends to increase due to the enhancement in the molecular collision as a result of the increased energy content of the gas, Whereas in liquids the viscosity decreases with the increase in temperature due to the weakening of the force of attraction between the molecules present in the liquid. On the whole, the higher the viscosity of a substance, the more resistance it will exhibit to the flow and thus will require more power to pump the fluid and transport it from one location to the other. Contrary to the Newtonian fluids, Non-Newtonian fluids do not display a linear relationship between the stress-strain rate and a deviation is observed as depicted in figure 3.4 which shows stress-strain curves for different Non-Newtonian fluid. It means that the apparent viscosity of the fluid defined as $(\tau/\dot{\gamma})$ is not constant and is a function of either τ or $\dot{\gamma}$. Additionally, the viscosity of some fluids also depends on the time period, and hence Non-Newtonian can be classified into two broad categories of time-dependent and time-independent fluids. Since our study is limited to modeling the hemodynamic of blood, which is a shear-thinning time-independent Non-Newtonian fluid, the discussion is restricted to just the time-independent fluids and these fluids can further be classified into shear-thickening, shear-thinning, and visco-plastic behaviour type.

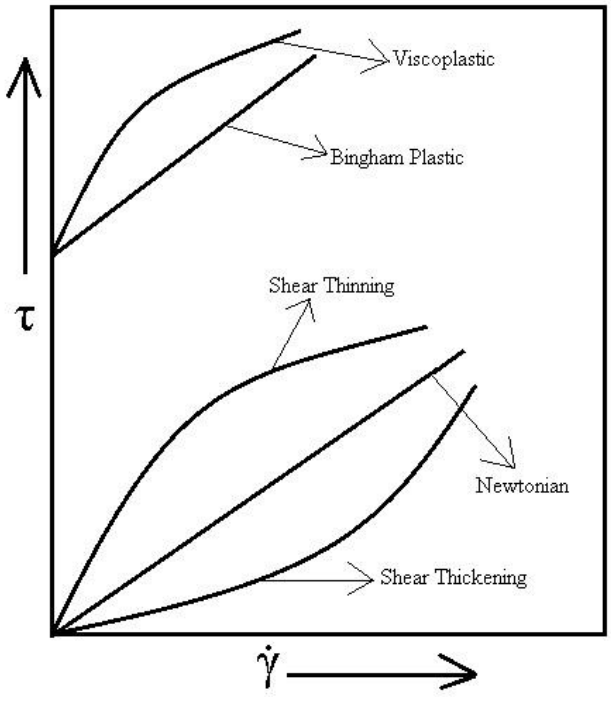

Figure 3.4 Qualitative curves for different types of fluids

The most common model employed to model the Non-Newtonian characteristics is the power-law model or also known as the Ostwald de Waele Equation given as

$$\tau = K(\dot{\gamma})^n \tag{3.13}$$

Where K is the consistency index and n is the power-law index. The apparent viscosity, η is obtained by dividing the shear stress with the rate of shear.

$$\eta = \frac{\tau}{\dot{\gamma}} = K(\dot{\gamma})^{n-1} \tag{3.14}$$

It is well understood that for 0< n<1, $\left({}^{d\eta}/_{d\dot{\gamma}}\right)$ will always yield a negative value which implies that with the increase of the shear rate, there will be a reduction in the shear stress component of the fluid. The fluids presenting this type of behaviour are termed as shear-thinning fluids. Smaller the value of n, more shear-thinning is the fluid. Blood, various polymer solutions, and suspensions like bentonite-in-water are good examples of shear-thinning fluids. However, when the value of n is greater than 1, the behaviour tends to reverse, i.e. with an increase in shear strain, the value of shear stress also increases. This type of fluids falls under the category of shear-thickening behaviour which can be readily witnessed in a corn starch and water mixture. For the case of n=1, the fluid showcase Newtonian rheology. The model employed to numerically understand the flow and mixing behaviour of blood in microchannels is the Carreau-Yasuda model as discussed briefly in the upcoming section

3.3.1 The Carreau-Yasuda model

In the present study, the Carreau-Yasuda model is used to capture the blood flow dynamics which have been extensively utilised by several researchers in the past [44], [46], [50]. According to the Carreau-Yasuda model, shear rate dependent viscosity is given by:

$$\eta(\dot{\gamma}) = \eta_0 + (\eta_0 - \eta_\infty)[1 + \lambda(\dot{\gamma})^a]^{{}^{(n-1)}/_a} \tag{3.15}$$

Where η_∞, η_0, λ, n and a are infinite shear rate viscosity, zero shear viscosity, characteristic relaxation time, flow index, and an empirical constant, respectively. Here, η_o = 0.1600 Pa-s, η_∞= 0.0035 Pa-s, λ = 8.2 s, a= 0.64 and n= 0.2128. All the values are referred from the previous work of Abraham et. al. [47]. Further, $\dot{\gamma}$ denotes the scalar shear rate given by:

$$\dot{\gamma} = \sqrt{2 \times (D : D)} \tag{3.16}$$

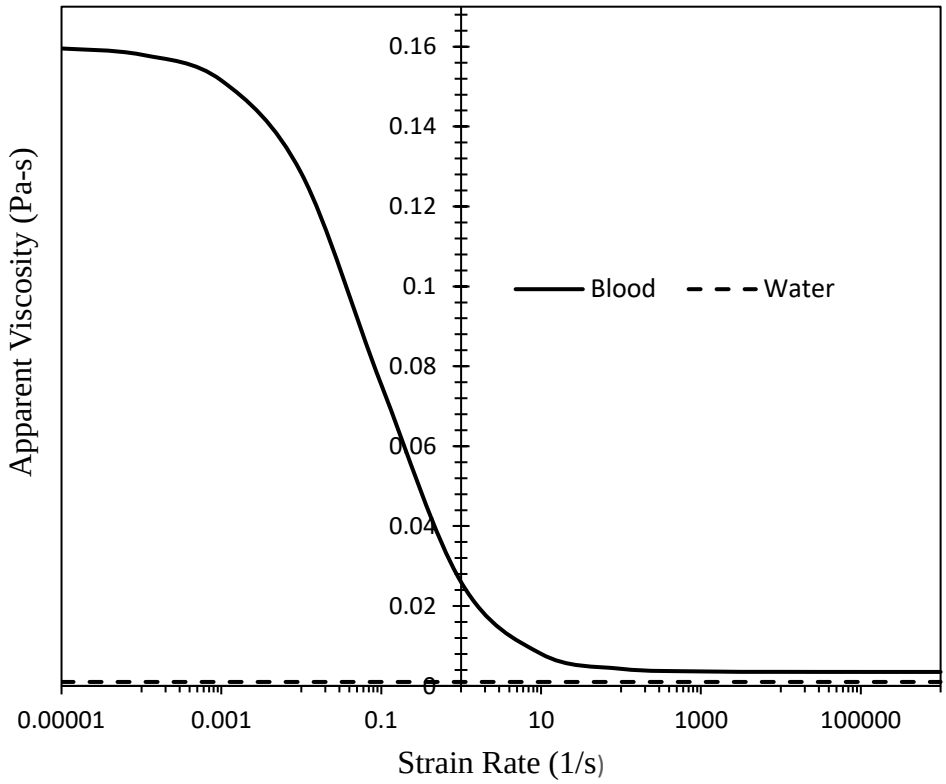

Figure3.5 Variation of the apparent viscosity of blood and water with strain rate

Where D is the rate of deformation tensor. The model is continuous at all the positive values of shear strain rate and as seen in figure 3.5, the apparent viscosity of blood behaves as Newtonian fluid for both very high and very low shear strain rate. At very low mass loading ($\dot{\gamma} \leq 0.001$), the blood is highly viscous ($\eta_o = 0.1600$ Pa-s) relative to the constant viscosity of water (0.001 Pa-s) whereas at higher values of strain rate or high mass loading the apparent viscosity of blood is appear to be close to the constant viscosity of water (0.001 pa-s) and appears to be asymptotic but a significant difference in viscosities (0.0025 Pa-s) are observed between water and blood at a lower value of strain rate.

3.4 Numerical Solution method

The flow domain of the micromixers is generated using the readily available CAD modeling software Solidworks. The modeled flow domain is then discretized into small

elements and solved numerically using the CFD solver of ANSYS fluent which employs finite volume method. This section discusses the coupling and discretization schemes, boundary conditions, and properties of the fluids used to solve the discretized equations.

3.4.1 Coupling and spatial discretization schemes

The steady-state laminar flow model and species transport model in ANSYS fluent are turned on to understand the flow and mixing behaviour. The second-order upwind scheme is used to discretize the continuity, momentum & species transport equations and the SIMPLEC algorithm is employed for the pressure-velocity coupling. The residual values for all the equations are set to 10^{-8} as the convergence criterion. Table 3.2 presents a summary of the numerical schemes employed in the computational simulations when blood is the working fluid.

Table 3.2 Numerical schemes used for CFD solutions

Pressure-velocity coupling	**SIMPLEC**
Pressure	Second-order
Gradient	Least squares cell-based
Momentum	Second-order upwind
Species	Second-order upwind

3.4.2 Boundary Conditions

The following boundary conditions are used to solve the above-mentioned equations. In the case of Newtonian mixing, water enters inlet 1 with species concentration ‘one’ and water-dye solution enters inlet 2 with species concentration specified as ‘zero’. Velocity at both the inlets is specified based on Reynolds number, Re.

$$Re = \frac{\rho V_m D_h}{\mu} \tag{3.17}$$

Where, V_m is the mean velocity of the flow, D_h is the hydraulic diameter of the microchannel, and ρ is the density of the fluid.

No-slip and zero wall flux conditions were given to the walls of the micromixer. Zero specific pressure is specified at the outlet of the mixer. For Non-Newtonian mixing, blood

enters from both the inlets with species concentration ‘one’ and ‘zero’ respectively and the velocity inlets are computed based on the total mass flow rate inside the main mixing microchannel. All the other boundary conditions are the same as for the case of Newtonian mixing.

3.5 Quantification of Mixing

To examine the mixing performance of the two micromixers, a variance-based method is used to compute the mixing index to quantify the mixing process on a plane as used by various researchers[29-32]. The mixing index is given by

$$Mi = \left(1 - \sqrt{\frac{\sigma^2}{\sigma_{max}^2}}\right) \times 100 \tag{3.18}$$

$$\sigma^2 = \frac{1}{n}\sum_{i=1}^{n}\left(c_i - c_{avg}\right)^2 \tag{3.19}$$

Where, σ^2 is the actual variance in the mass fraction of the fluid component and σ_{max}^2 represents the maximum variance. c_i is the mass fraction at sampling point i, and c_{avg} is the average value of the concentration of the fluid at a cross-section considered for the calculation. For mixing involving two equal streams of fluid, the value of σ_{max}^2 is calculated to be 0.25. n is the total number of points considered on the plane, a high value of n improves the accuracy of the solutions and thus, in current study n is taken to be 900. The mixing index/efficiency (Mi) varies between 0 and 100, 0 signify no mixing has taken place whereas 100 is the best case representing complete mixing of the fluids.

3.6 Grid generation and sensitivity analysis

Grid generation is a crucial step in a CFD study. The quality and size of the elements used to divide the flow domain have a huge impact on the numerical results and its accuracy. Coarse mesh takes less computational time but has poor numerical prediction capability whereas fine mesh is proven to give better accuracy with higher computational time. Thus, selecting an optimized grid element size is necessary keeping both the accuracy and the computational time in mind. A grid sensitivity analysis is performed to observe the variation of variables like velocity, pressure drop, and mixing index with a change in

the number of elements or the grid size. The geometry of the fluid domain of both the types of micromixers is modeled in the CAD Solid works software, whereas the ANSYS meshing module is used to generate the grid with tetrahedral elements as shown in figure 3.6.

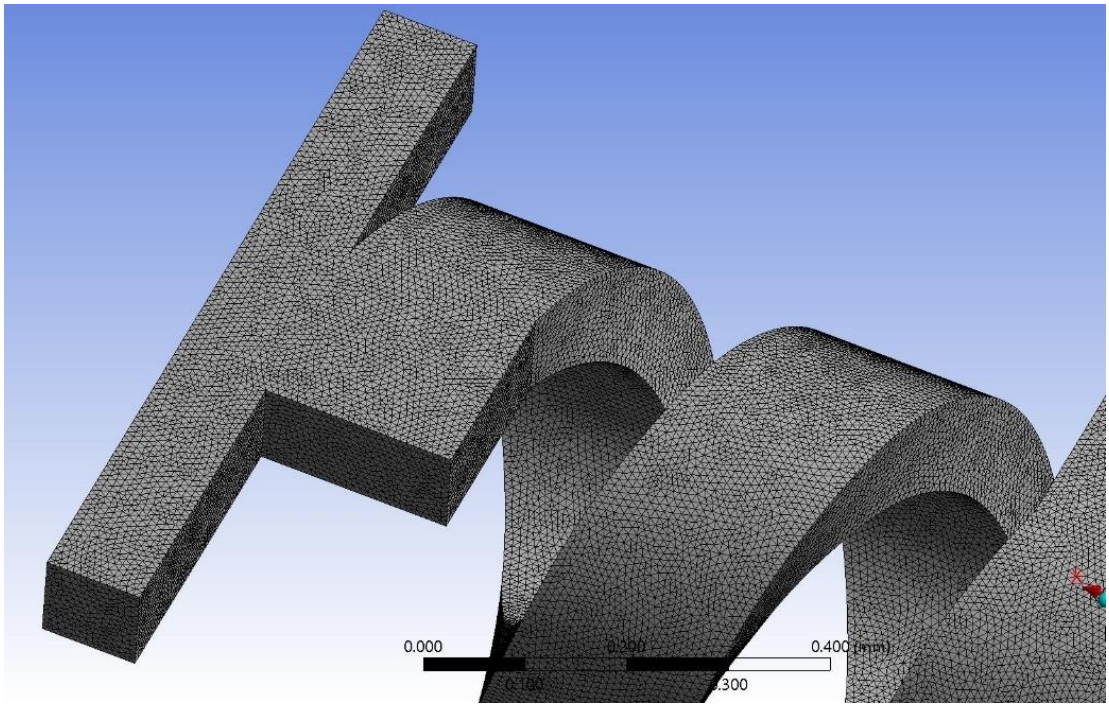

Figure 3.6 Mesh of TDHM with 1 million tetrahedral elements

These elements are used for meshing due to the complexity of the flow domain in the case of TDHM. Figure 3.7 illustrates the variation of the mixing index and the pressure drop by increasing the number of elements in the flow domain. CFD simulations were performed for TDHM at a mass flow rate $\dot{m}$ = 0.0057 Kg/hr for Non-Newtonian fluid (Blood) to examine the behaviour of mixing index and pressure drop in the micromixer as the number of elements is increased. As shown in figure 3.7, the values of both the mixing index and the pressure drop seem to approximate to a fixed value after 2.55 million elements. There is a small difference of 0.35 % in the values of mixing index at 2.55 million and 4 million elements respectively. Therefore, this number is chosen to be the optimum number as further making the mesh finer will only increase the computational time and will require more power with almost the same results. Similar tests were carried out for all the cases before running the actual simulations. Furthermore, the variation of velocity at the centreline of the outlet section with the number of elements is depicted in figure 3.8 and it is seen that the velocity on different points at the centreline of the outlet section of the mixer doesn't change significantly after 0.42 million elements.

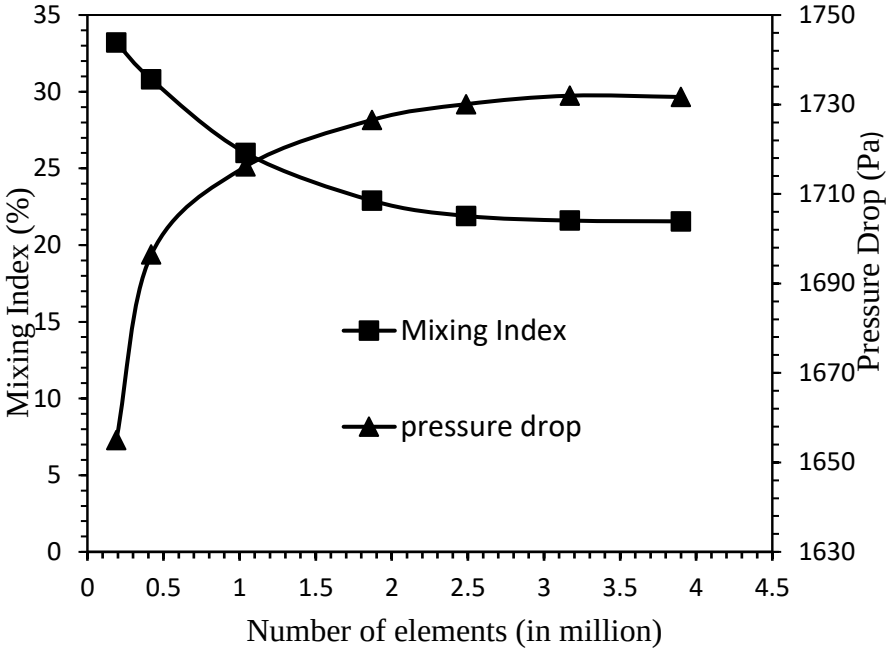

Figure 3.7 Grid sensitivity analysis

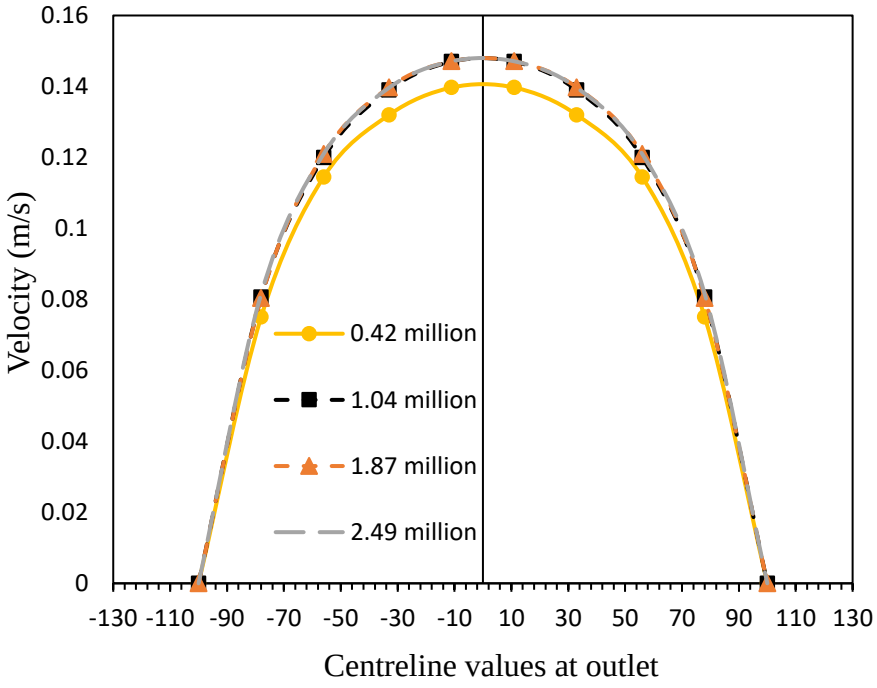

Figure 3.8 Variation of velocity at centreline of the outlet with the number of elements

3.7 Validation of the computational approach

Numerical solutions are accompanied by various types of errors making the solutions doubtful on its accuracy and thus validation of the computational results obtained is must with the experimental data or with the existing published research data. Two different working fluids (Newtonian and Non-Newtonian) are used in the study and hence two different validation tests are performed to check the accuracy of the picked approach before proceeding with actual simulations.

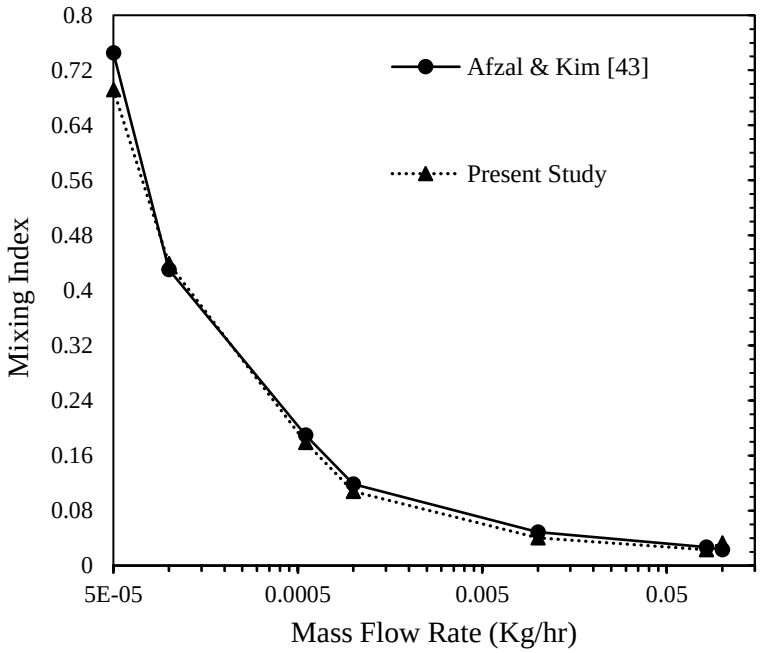

Figure 3.9 Mixing Index Comparison of the present study with the mixing index results of existing literature[43]

Afzal & Kim [43] performed numerical simulations to examine the performance of a serpentine channel micromixer and compared the results with the micromixer having a straight channel of length 4000 µm with a square cross-section of 100 µm × 100 µm. Working fluid is blood and the Carreau-Yasuda model was applied to study the rheology of blood at the micro-scale. Similar T-Micromixer is modelled and numerical simulations are performed under the same boundary conditions to ensure the reliability of the CFD approach. Figure 3.9 presents a comparison of mixing indexes obtained from the current study with that of the mixing indexes reported in the existing literature [43] at different mass flow rates of blood. The graph depicts that the current numerical results follow a

similar trend and a good agreement of results is visible with a maximum deviation of 4.72 % at the lowest value of mass flow rate.

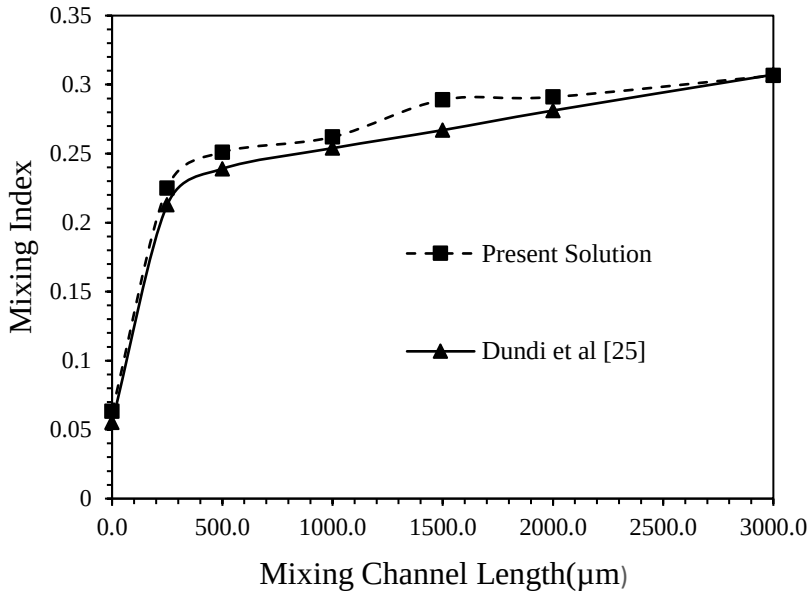

Figure 3.10 Mixing Index comparison of current T-mixer with that of the existing literature[25]

Another validation test was performed to ensure the accuracy of the numerical results when the working fluid is changed to water. Dundi et al. [25] evaluated the flow characteristics and mixing performance of water (Newtonian fluid) in a simple T-micromixer of length 3000 μm and proposed to improve the mixing performance by providing swirl components of velocity at both the inlets. The results of the mixing index obtained from the numerical simulations conducted using similar dimensions and under the same boundary conditions are compared with the results presented by Dundi et al. [25] at Re=266. Figure 3.10 illustrates the variation of mixing at different length of the channels measured from the T-junction for Re=266 and also provide a comparison between the present obtained results and the mixing index calculated in the existing literature. Furthermore, the contour representing the species concentration of water 1 (fluid 1) at the outlet plane is depicted in figure 3.11 and a similar trend is observed in the results of the mixing index proving the strength of the computational approach. Therefore, the prediction capability of numerical solutions can be further used to investigate the mixing performance in the case of TDHM.

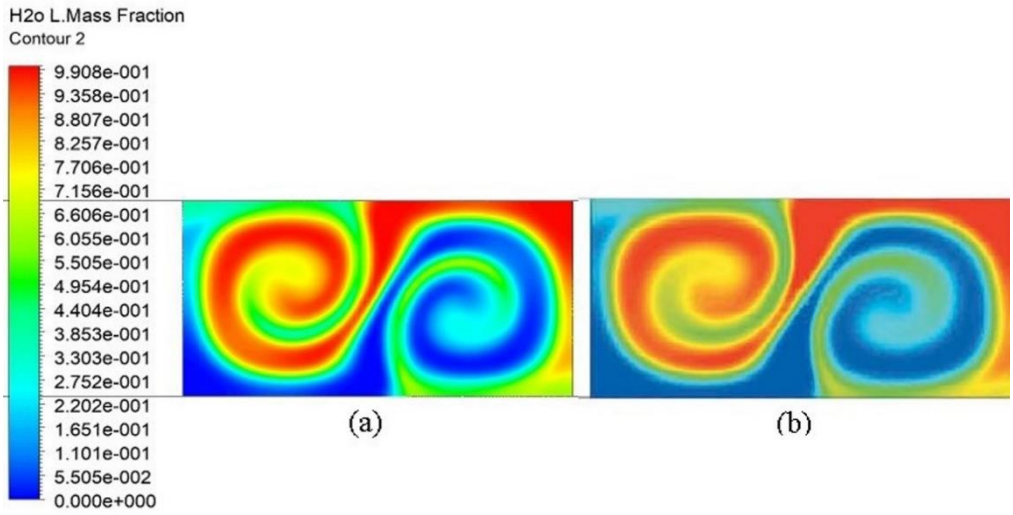

Figure 3.11 (a) Species concentration at the outlet of the current study. (b) Species concentration at the outlet for existing literature[25]

3.8 Summary

In this chapter, a brief explanation is presented of the mathematical modeling and governing equations used to examine the passive mixing performance of the micromixers. Also, the different approaches used for Newtonian fluid (water) and Non-Newtonian fluid (Blood) are described in detail. The consideration related to the CAD modeling of the TDHM and the meshing of the fluid domain is explained. Finally, the numerical solution techniques employed to obtain the mixing performance and the validation of this CFD approach is done using the data found in the existing literature.

CHAPTER 4

RESULTS AND DISCUSSIONS

The current chapter provides a thorough discussion of the numerical results obtained for both Newtonian fluid and Non-Newtonian blood in STM and TDHM. This chapter is divided into three major sections. The first section provides information on the mixing performance and flow characterization in a simple T-micromixer (STM) which has a straight channel for both water and blood as the working fluids. The second section includes numerical results of a 3-dimensional helical micromixer (TDHM) with the peripheral length of the spiral equal to the length of the STM to showcase the comparison. Lastly, section three deals with the performance evaluation of TDHM having the axial length equal to that of the STM and

4.1 Mixing and flow analysis in Simple T-micromixer (STM)

As discussed in chapter 3, the total length of the straight mixing channel is 3000 μm with a cross-sectional area of 200 × 100 μm. It is important to note that the axial distance and the peripheral mixing length in a STM are equal whereas it differs for the case of TDHM due to the introduction of 3-dimensional curvature. Flow and mixing behaviour of Newtonian and Non-Newtonian fluid (Carreau-Yasuda model) in a STM is discussed in section 4.1.1 and 4.1.2, respectively.

4.1.1 STM with Newtonian fluid (water) as the working fluid

Several experimental and numerical work is available for STM describing the three types of flow regimes, that are diffusion regime, vortex regime, and the engulfment flow when the working fluid exhibit Newtonian characteristics [16], [22], [51]. Similar behaviour is observed in the current study with water which is a Newtonian fluid. For low Reynolds number i.e. below 15, the streamlines in the flow appear to be straight and parallel as seen in figure 4.1 (a) with no sign of vortex formation in this range and thus is termed as the laminar diffusion regime since the sole mode of mass transfer, in this case, is the molecular diffusion occurring at the interface of the two fluids. As the Reynolds number is raised further, weak vortices are visible which are symmetrical about the vertical plane

at the center of the cross-section of the T-junction for Re≥40 as seen in figure 4.1 (b) and thus,

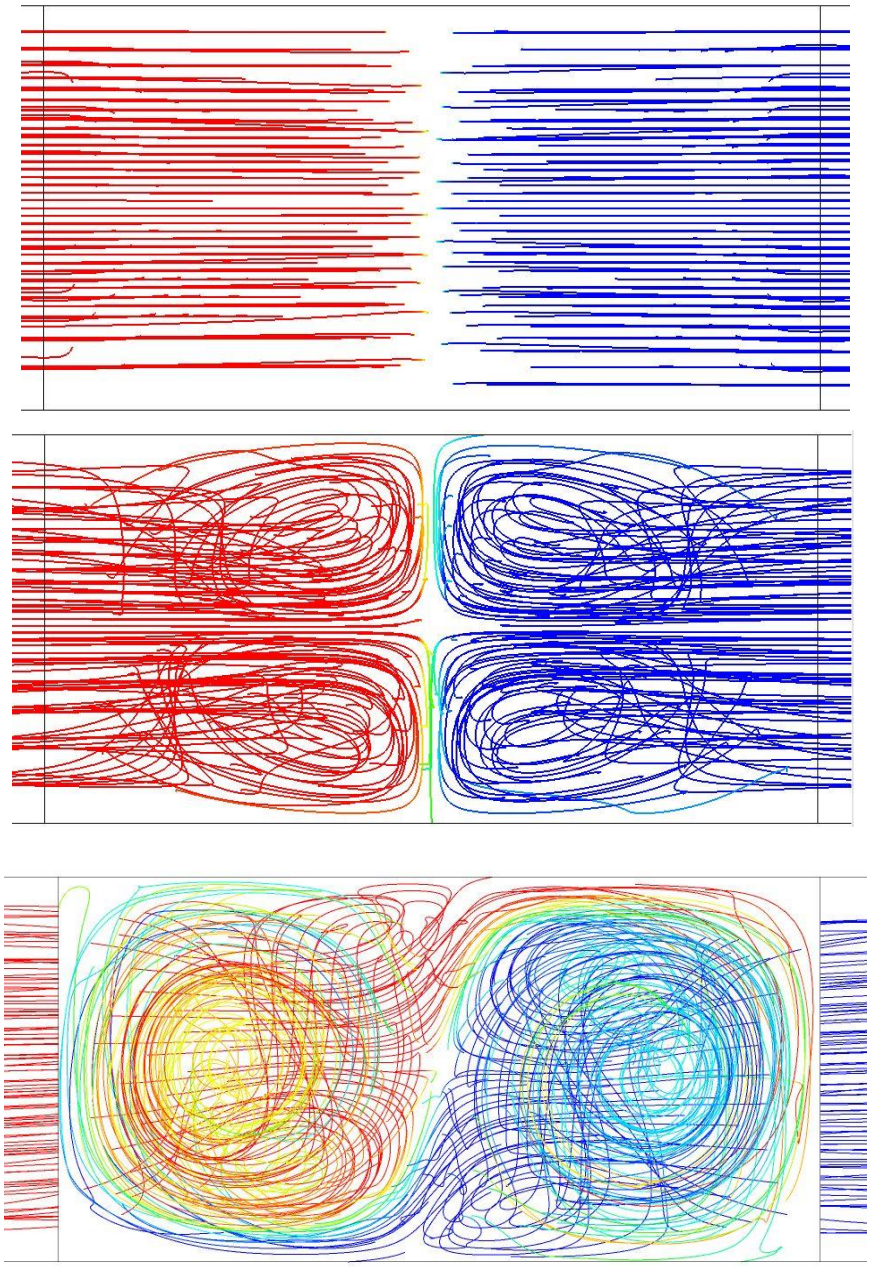

Figure 4.1 Streamlines for water in simple T-micromixer when viewed from the outlet at (a) Re=10 (b) Re=106 and (c) Re=266

this regime is known as the Vortex regime. Although vortices are formed, there is no significant improvement in the mixing because, with an increase in the Reynolds number, there is a reduction in the residence time of fluids causing the mixing efficiency to drop further. This regime continues up to Re=170, after which both the fluid breaks the

symmetrical vortices and penetrate into each other as seen in figure 4.1 (c) resulting in an advancement of chaotic advection and thus a sharp jump in the mixing index is observed in this regime called as the engulfment regime or the engulfment flow zone. The streamlines are no more parallel or symmetrical as observed in the case of laminar diffusion and laminar vortex regimes, respectively. The characterization of the three types of regimes and the variation of mixing performance with the Reynolds number is depicted in figure 4.2 and it is seen there is a sudden rise in the mixing index as the flow enters in the range of engulfment flow.

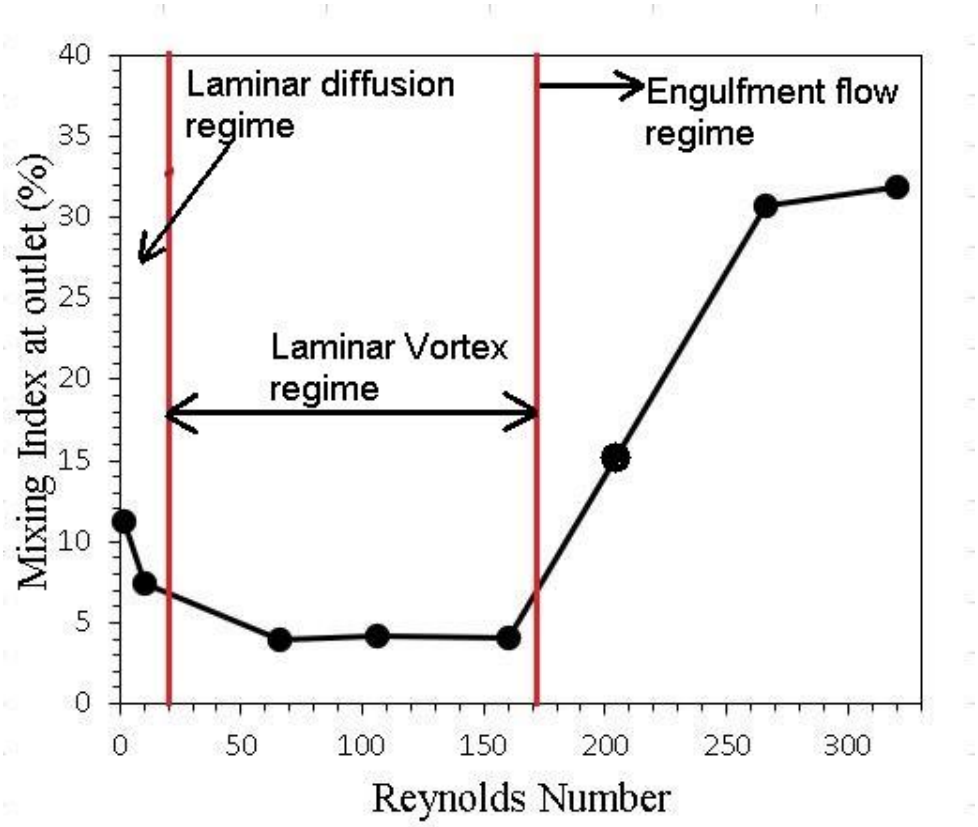

Figure 4.2 Flow characterization and the effect of Reynolds number on the mixing performance of the water in STM.

4.1.2 STM with Non-Newtonian blood as the working fluid

The flow characteristics observed in the case of Non-Newtonian fluid are different from the flow behaviour for a Newtonian fluid. For the major portion of the mass loading of blood in straight channel ranging from 5×10^{-5} Kg/hr to 5.5×10^{-2} Kg/hr, the streamlines of the flow appear to be straight, parallel and well-organized as seen in figure 4.3 (a) signifying that the mass transport is purely governed by the diffusion phenomenon and this range is termed as the laminar diffusion regime. The increase in mass flow rate causes

a reduction in the time of contact available for the molecular diffusion to occur, thus reducing the mixing index. After $\dot{m}$= 5.5 × 10^{-2} Kg/hr, vortices of weak strength are

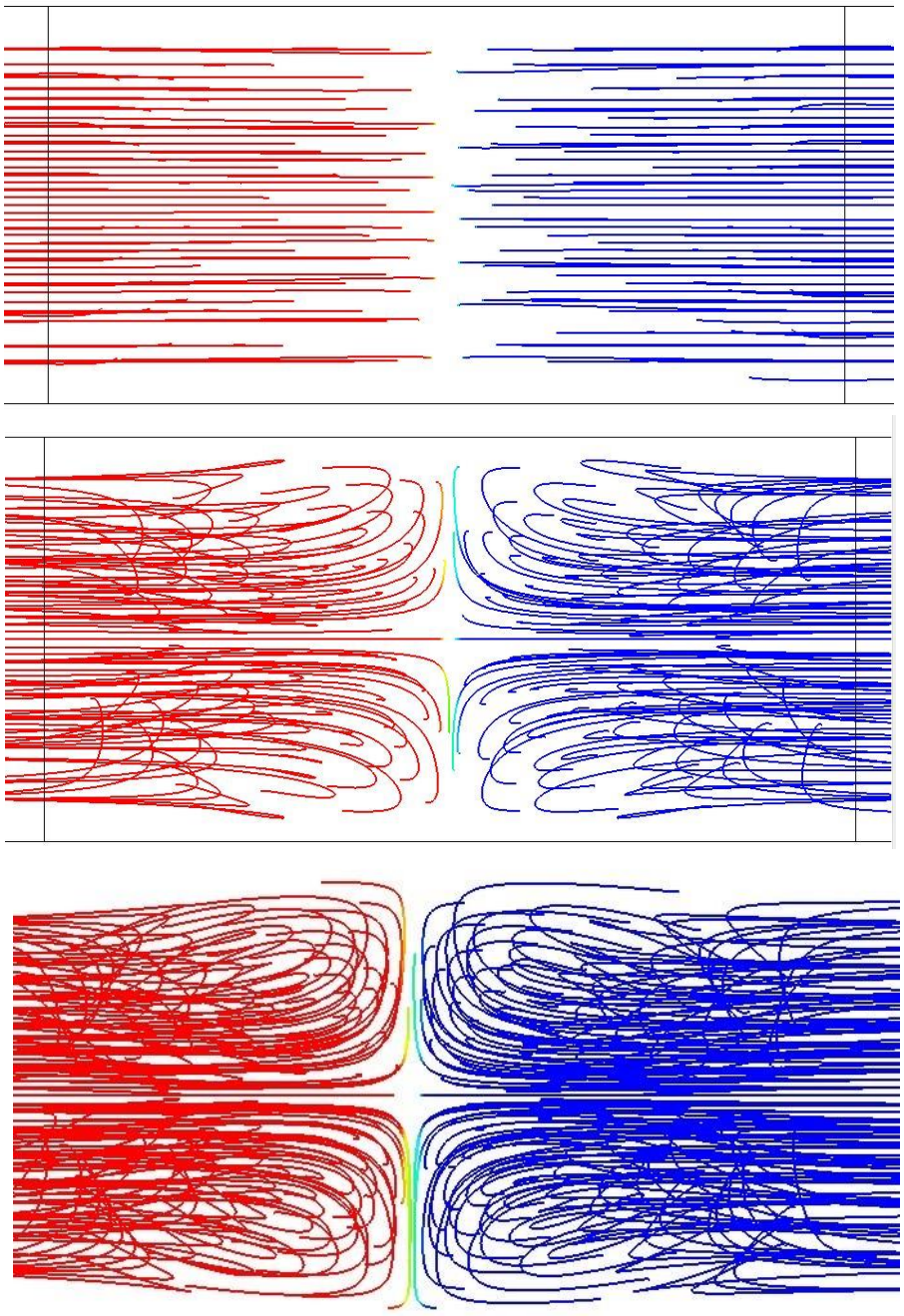

Figure 4.3 Streamlines based on species concentration for blood in STM at ṁ = (a) 1.4 × 10^{-3} Kg/hr (b) 0.06094 Kg/hr and (c) 0.15227 Kg/hr

identified which are symmetric about the vertical axis as seen in figure 4.3 (b) &(c) and these vortices don't seem to have any impact on the mixing performance and therefore mixing is still dominated by diffusion in this vortex regime. The secondary flow characteristics bear distinctive nature in Blood (Non-Newtonian) and water (Newtonian)

fluids. Secondary flow in the case of Newtonian fluid enter the engulfment zone with an increase in the Reynold number, Re as visualized in figure 4.1(c) whereas no engulfment flow regime is seen in the case of blood at a corresponding mass flow rate of 0.15227 Kg/hr [figure 4.3 (c)] and the strength of secondary flow is weak leading to a drop in mixing index when compared to the mixing index of water. The higher viscosity of blood dampens the vortices formed at high mass loading and thus the strength of the secondary flow appears to be diminishing when the working fluid is blood. Figure 4.4 depicts the continuous decreasing pattern of the mixing index with an increase in the mass flow rate of blood with flow regimes.

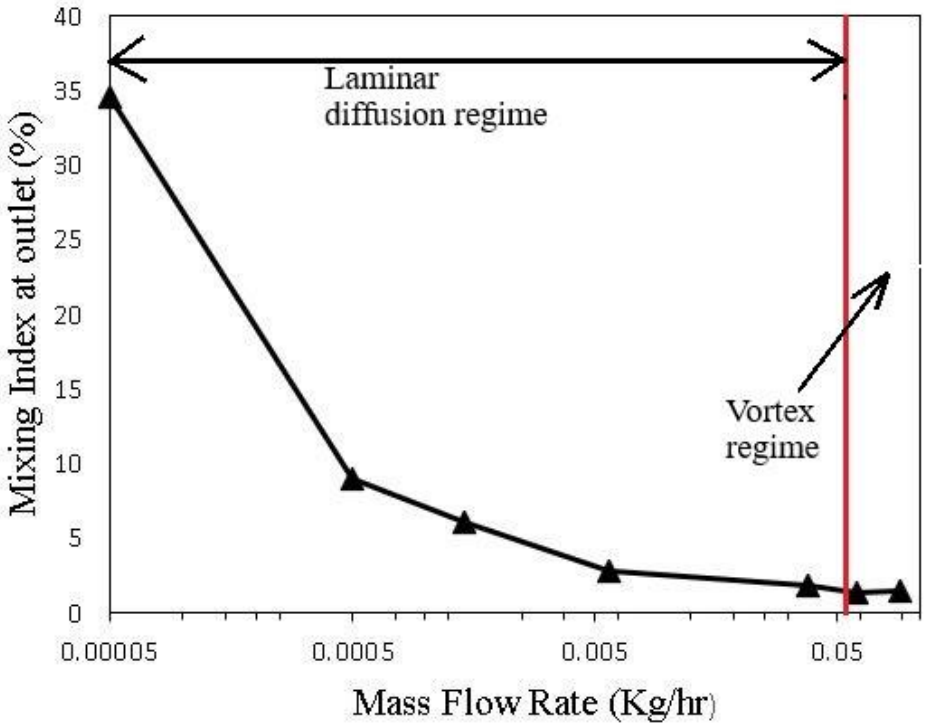

Figure 4.4 Effect of mass flow rate of blood on the mixing index at outlet for the conventional STM

4.2 Mixing and flow analysis in 3-dimensional helical micromixer (TDHM) with same mixing length as that of STM

Numerous works on spiral channels bearing different shapes and sizes present effective mixing within a short distance making the mixer compact [34], [52], [53]. Additionally, the three-dimensional shape of the mixing channel creates rotation as the fluid flows in the channel leading to advection between the fluids, and thus three-dimensional helical shape is selected to investigate the mixing performance of non-Newtonian blood. This section provides information on the mixing performance of the TDHM and compares the

obtained results with the mixing performance in a straight channel of STM. The mixing length or the peripheral length of the TDHM, in this case, is kept equal to the length of the STM, i.e. 3000 µm. However, the axial length corresponding to the peripheral length of 3000 µm is calculated from equation 3.1 as 741.14 µm with 2 number of turns of the helical microchannel. The first part of this section deals with the Newtonian fluid whereas the second part discusses the performance and flow when the working fluid is changed to the Non-Newtonian blood.

4.2.1 TDHM (same mixing length) with water as the working fluid

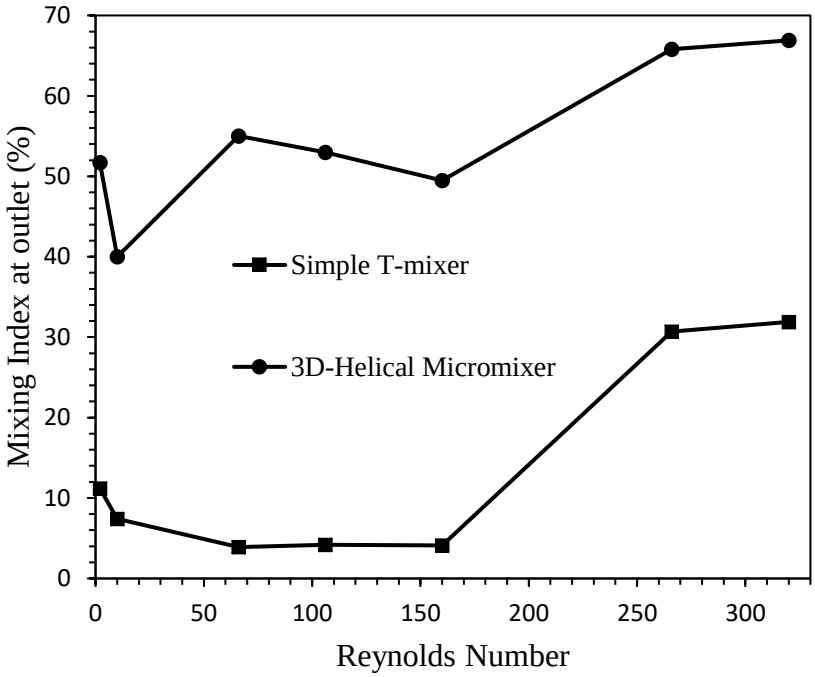

Figure 4.5 Pattern of mixing index of STM and TDHM with the increase in Reynolds number for a Newtonian fluid

Figure 4.5 represents a comparison of the mixing index at the outlet of simple T-micromixer (STM) and 3-D helical micromixer (TDHM) for a wide range of Reynolds numbers ($2 \leq Re \leq 320$) with water (Newtonian fluid) as the working fluid inside the channels. At low Reynolds number, the mixing process reported in STM is very poor due to the straight laminar flow nature of species resulting in low mass diffusion phenomenon. The mixing index further shows a reducing trend up to a point defined as the 'critical Reynolds number', after which the flow enters into the engulfment zone where the intensity of vortex increases and thus there is an enhancement in the mixing phenomenon

of the fluids due to chaotic advection. Critical Reynolds number is the point where the transition from molecular diffusion to the chaotic advection takes place and with an increase in the Reynold number after this point, the secondary flow grows in strength.

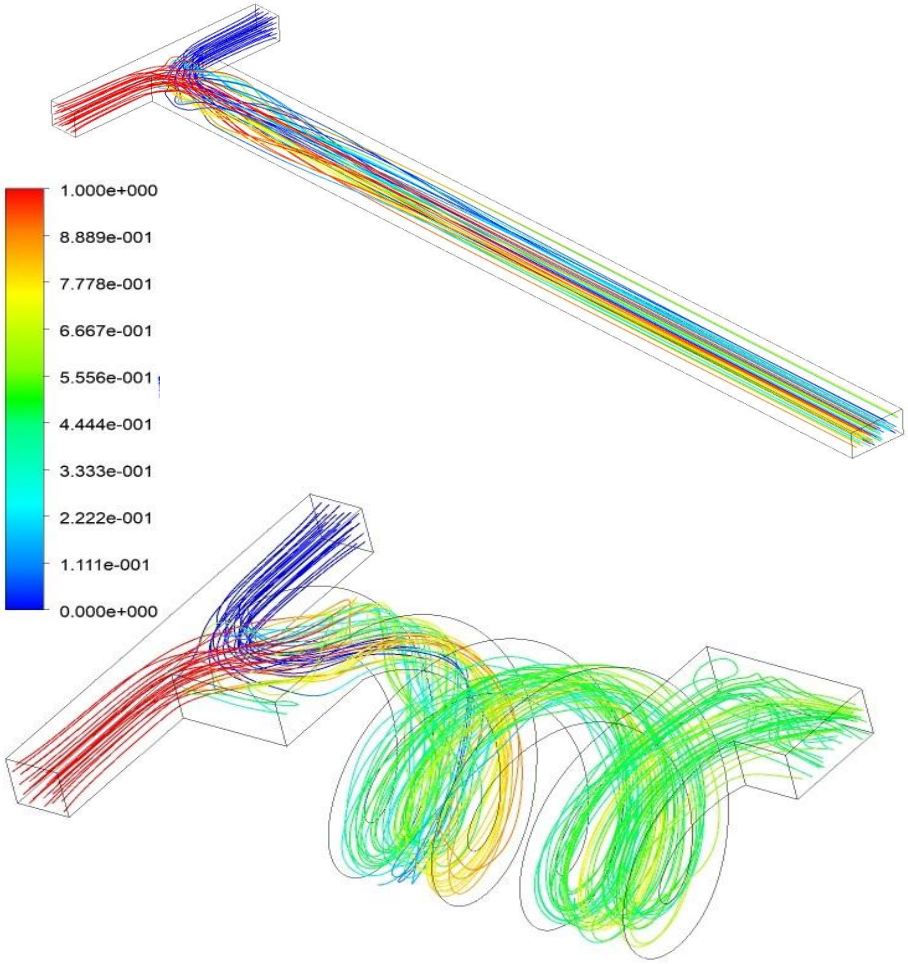

Figure 4.6 Streamlines based on species concentration along the length for (a) STM (b) TDHM at Re=266

TDHM seems to be a better option due to its higher mixing performance at all the values of the Reynolds number as compared to the STM (figure 4.5). At low Reynolds number, TDHM increases the interfacial area between the fluids and stretches the fluids leading to enhancement in mass diffusion. At higher Reynolds number (Re ≥150), the flow is dominated by secondary flow created due to the centrifugal force imparted as a result of the three-dimensional curvature design of the TDHM and thus the chaotic advection is introduced which significantly enhances the mixing process. This phenomenon can be visualized by the velocity streamlines based on the concentration of species for STM and TDHM as shown in figure 4.6 (a) & (b) respectively at Re=266. A further study was

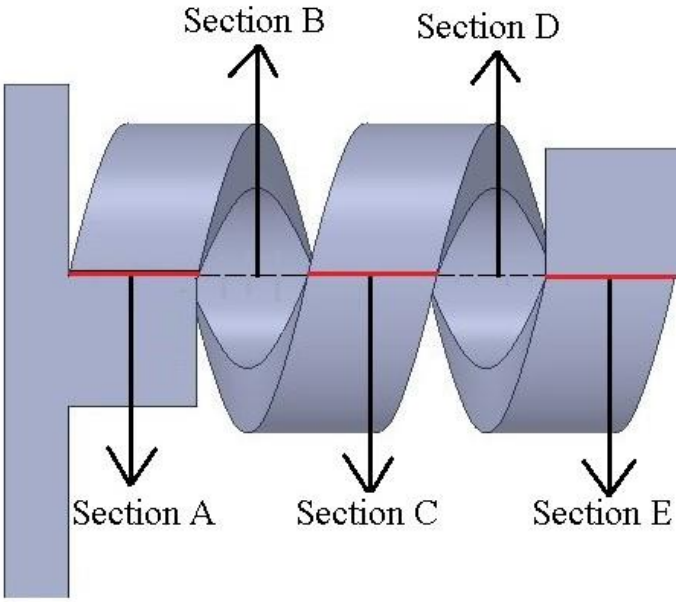

Figure 4.7 Locations of various sections A, B, C, D & E considered for study

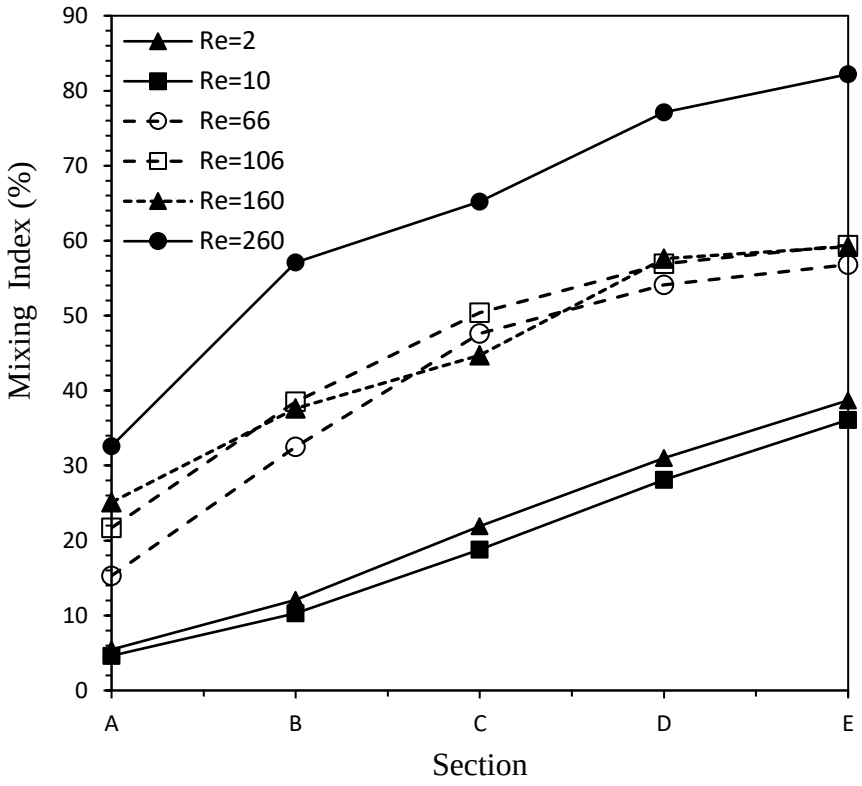

Figure 4.8 Variation of mixing index at five different sections along the length of the TDHM for Newtonian fluid

performed to examine the variation of the mixing index of TDHM at various section length (refer figure 4.7) considered along the flow direction as shown in figure 4.8. For Re = 2 & 10, the mixing curve appears to be linear in nature, however rapid mixing of fluid takes place within a short distance at high values of Reynolds number. At Re=260,

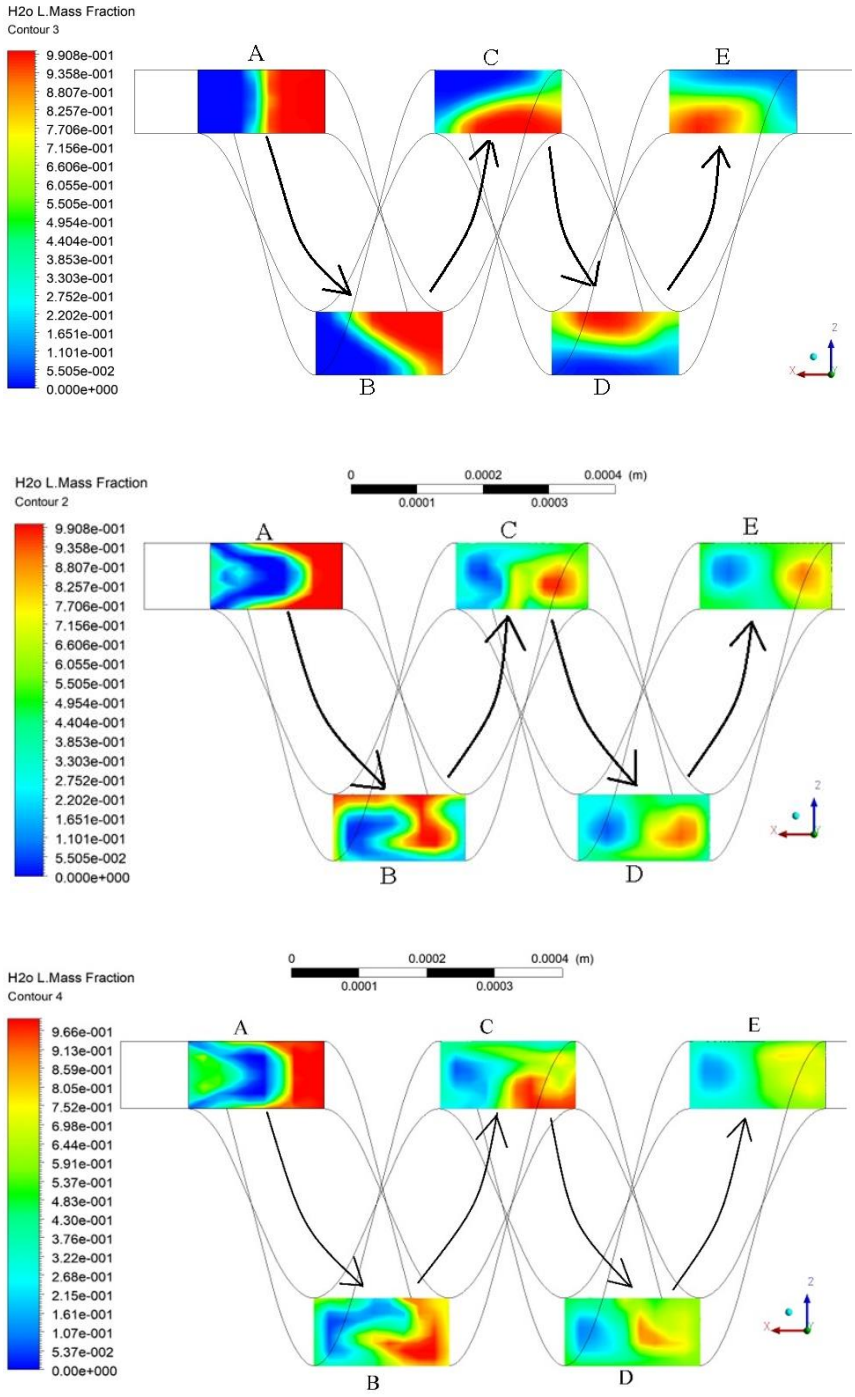

Figure 4.9 Concentration of species at different sections along the length of TDHM for Re=(a) 2, (b) 60 and (c)160

the mixing index sharply rises from 32.6% at plane A to 82.2% at plane E indicating the advantage of employing TDHM even for high Reynolds number flow. Figure 4.9 represents the concentration of species at planes A, B, C, D and, E of TDHM for Re =2, 66 &160. For Re=2, the interface between the two fluids appears straight and thin on initial planes A& B (figure 4.9) but as the flow, progresses to plane C and beyond, the interface bends and grows thicker in size. At higher Reynolds number (Re = 66 & 160),

the inertia of fluid tends to impart rotation to the fluid leading to stretching and increase in strength of the vortices which enhances the mixing process.

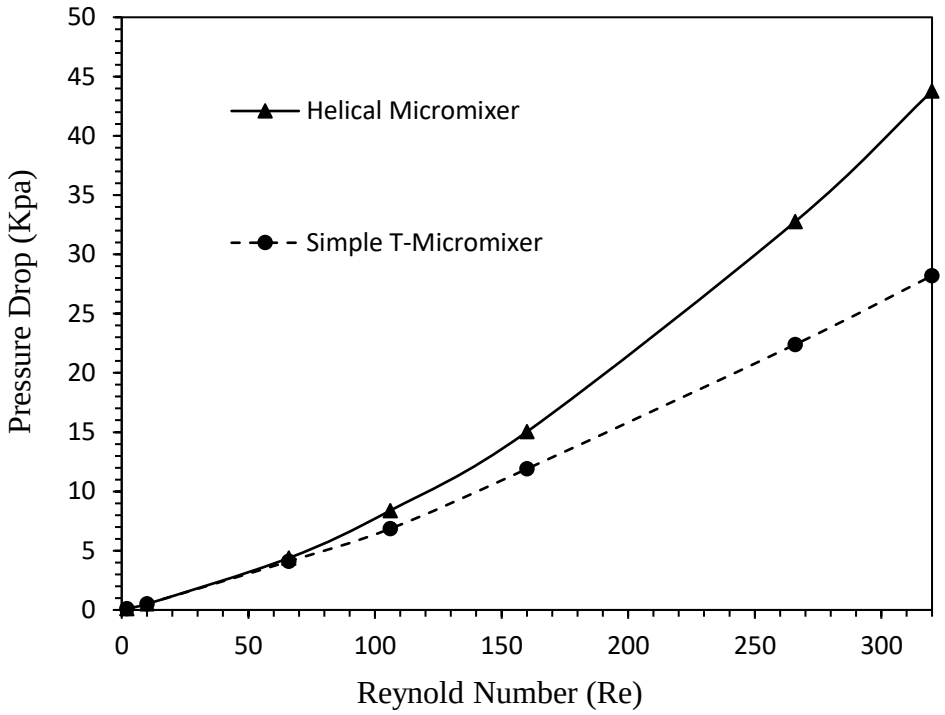

Figure 4.10 Variation of pressure drop with Reynolds number for STM and TDHM with water

The enhancement in mixing always comes with the increase in pumping power to drive the flow in the microchannels, this becomes more significant in the case of passive micromixers. Thus, it becomes essential to investigate the pressure drop in the micromixers which is directly linked with the requirements of input energy. A comparison of the change in pressure between inlets and outlet of STM and TDHM with increasing Reynolds number is represented in figure 4.10. No noticeable difference is seen in the pressure drop for Reynolds number less than 66. However, TDHM pressure drop line promptly deviates from the pressure drop line of STM as the Reynolds number is increased with the highest difference obtained at the Re=320.

4.2.2 TDHM (same mixing length) with Non-Newtonian blood as the working fluid

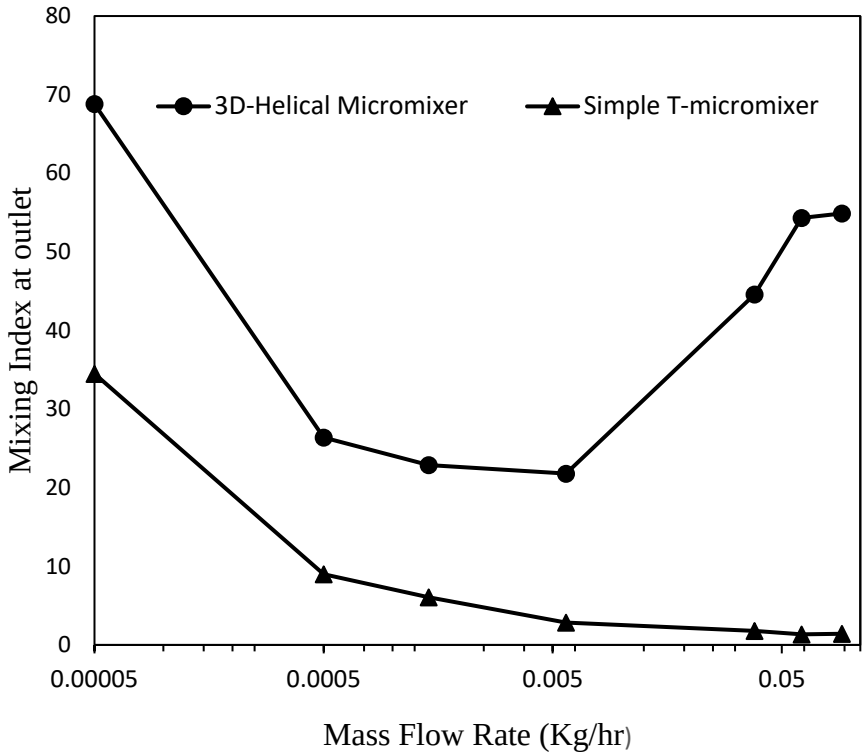

Figure 4.11 Effect of the mass flow rate of the blood on the mixing index at the outlet in simple T-micromixer and 3D-Helical micromixer with Non-Newtonian blood

The variation of the mixing index at the outlet of Simple-T mixer (STM) and TDHM for the Non-Newtonian fluid with the mass flow rate of the blood is shown in figure 4.11. At low mass flow rates, the mixing process is dominated by diffusion mass transport of molecules but due to the higher residence time, good mixing is achieved in both STM and TDHM as the fluids remain in contact for a longer period while flowing through the channels. However, TDHM performs better than STM even at low mass flow rate because of the interface perturbation i.e. stretching & folding of fluid layers in the case of TDHM which is absent in a simple straight channel of STM. A noteworthy difference of 34.3 % is noted at the lowest mass flow rate $\dot{m}$ =0.00005 Kg/hr in the mixing index of STM and TDHM. Further increase in the mass flow rate results in a reduction of residence time and thus a drop in mixing index is witnessed due to lower diffusion mass transport as seen in figure 4.12 (a), (b) & (c), which represents the three-dimensional streamlines based on the species concentration in STM (left) and TDHM (right) for m= 0.00005 Kg/hr, 0.0057

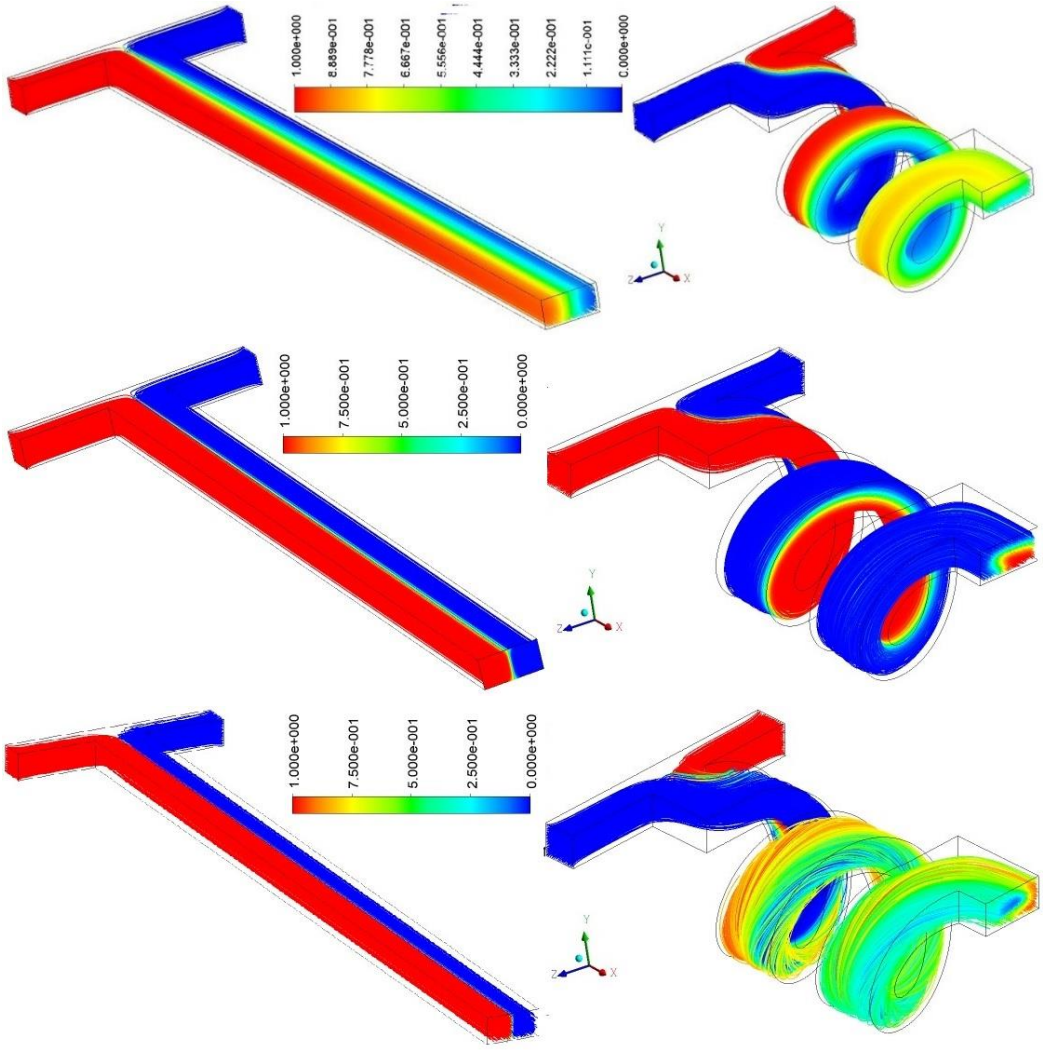

Figure 4.12 3D-Streamlines with variation of species concentration along the length for STM (left) & TDHM (right) for (a) $\dot{m}$ =0.00005 kg/hr (b) $\dot{m}$ =0.0057 kg/hr (c) $\dot{m}$ =0.0914 kg/hr

Kg/hr & 0.0914 Kg/hr, respectively. STM records a continuous drop pattern in mixing index with increasing mass flow rate, whereas a decreasing-increasing trend is seen for TDHM. This is because after reaching the lowest mixing performance, the flow in TDHM is dominated by the chaotic advection phenomenon introduced due to the three-dimensional curvature and therefore a sharp rise in mixing is seen with the further increase of mass flow rate of the blood, $\dot{m} \geq 0.006$ Kg/hr that can be visualized in figure 4.13 (a) & (b), which depicts the concentration of species at the outlet for different mass flow rates in STM (left) and TDHM (right), respectively. Afzal & Kim [50] studied the mixing and flow patterns in the straight and a serpentine channel for Non-Newtonian fluids. A steep reduction was

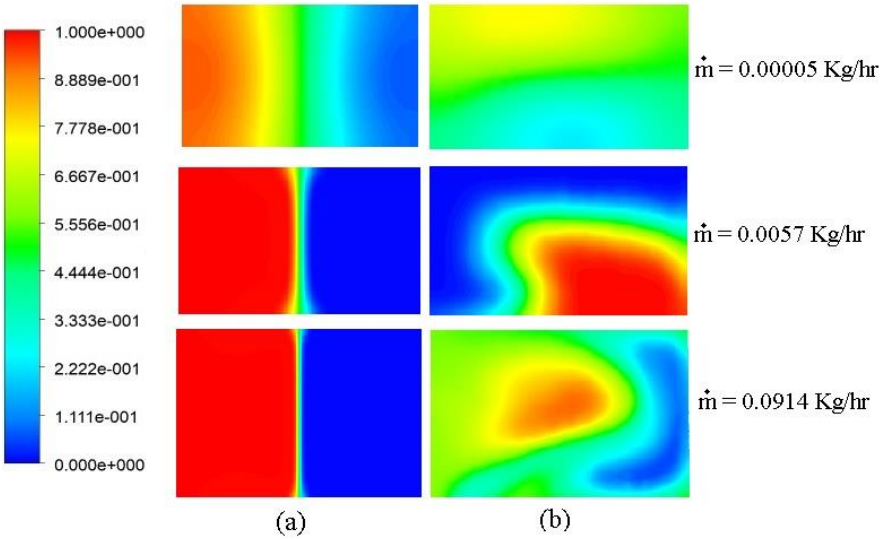

Figure 4.13 Species Concentration at outlet for (a) STM (b) TDHM

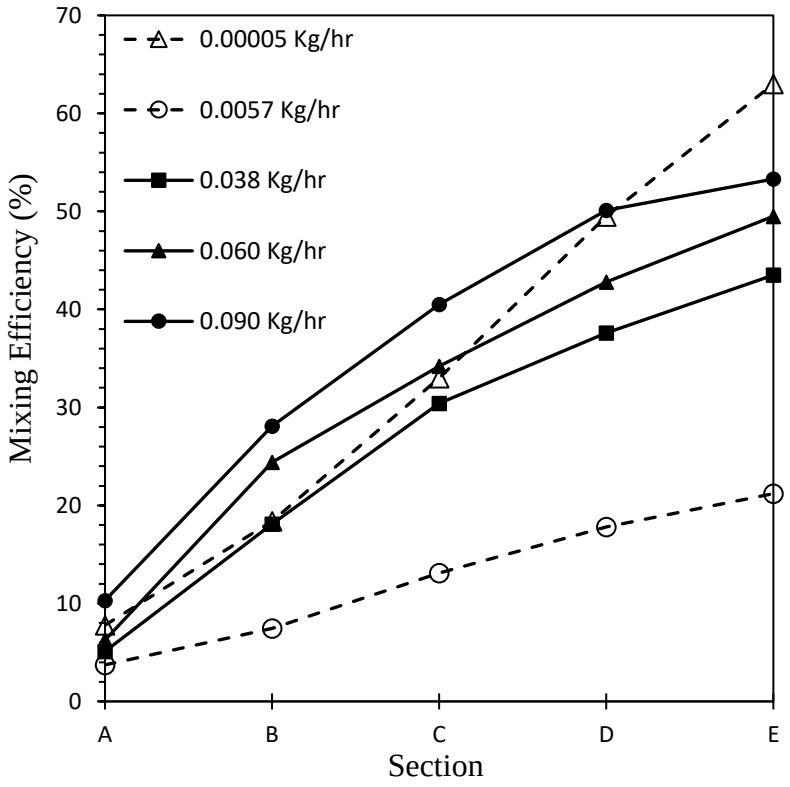

Figure 4.14 Pattern of mixing index at five different locations along the length of the TDHM with blood

observed in the mixing efficiency for the case of serpentine mixer having blood as the working fluid with minimum value well below 5%, however, our design proposes an efficient mixing with minimum mixing index of 21.8% observed at $\dot{m}$ = 0.0057 Kg/hr. To get a deeper insight into the mixing process in the effective TDHM, mixing index at 5 different sections along the length (figure 4.7) of the mixer was calculated for a wide

range of mass flow rates as shown in figure 4.14. The mixing efficiency increases linearly with the distance from the inlet and a sharp rise were seen between section A and section E for the smallest value of mass flow rate considered in the study ($\dot{m}$= 0.00005 kg/hr).Overall, the TDHM carries numerous advantages over the STM from the mixing performance point of view.

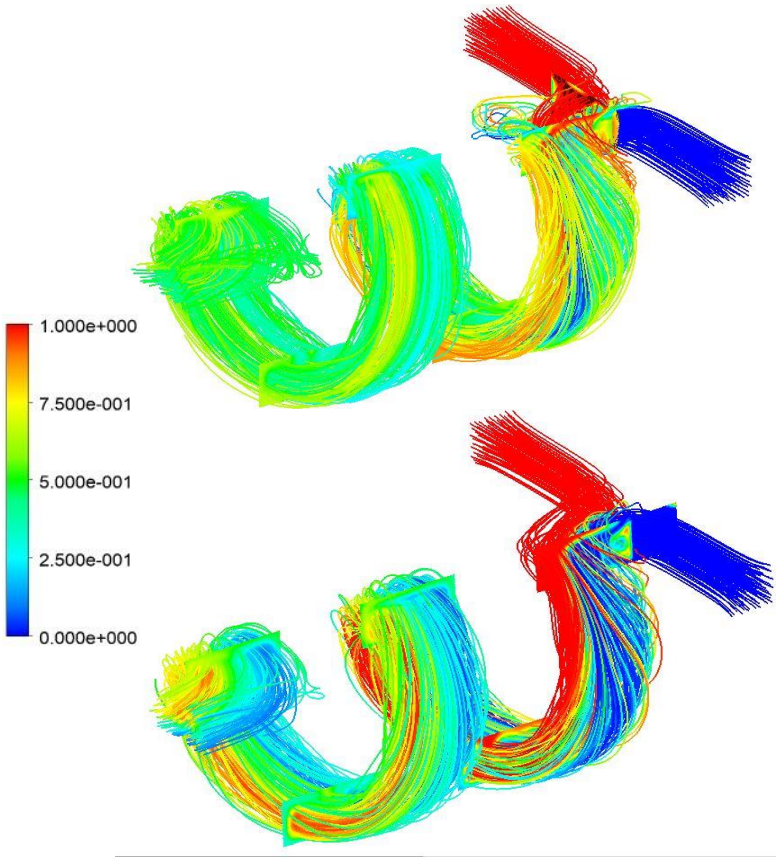

Figure 4.15 Streamlines based on the species concentration for (a) Water at Re=266 and (b) blood at ṁ=0.1522 Kg/hr (for corresponding Re=266)

The difference in the mixing performance when the working fluid is changed from water to blood can be understood with the visualization of streamlines in the microchannel. At low Reynolds number of 2 for water and the corresponding mass flow rate of 1.14×10^{-3} Kg/hr for blood, the flow appears to be well aligned with the helical walls of the mixer and molecular diffusion is the sole type of mixing. With an increase in the Reynolds number to Re=266 and the $\dot{m}$= 0.1522 Kg/hr for blood, chaotic advection is visible for both blood and water as seen in figure 4.15. However, closer observation reveals that the strength of vortices and secondary flow is more in the case of water due to its lower

viscosity (0.001 pa-s) when compared to blood (η_∞ =0.0035) at high shear rate. The lower viscosity produces lesser magnitude of viscous forces thus promoting the rotation and formation of vortices in water, while the high viscosity of blood results in a higher magnitude of viscous forces reducing the strength of the secondary flow. Figure 4.16 illustrates the variation of pressure drop in the microchannels of STM and TDHM with the mass flow rate of the fluid. At low mass flow rates, there is no notable difference in the pressure drop of the two micromixers. However, with an increase in the mass flow rates, TDHM shows a steeper rise in the pressure drop owing to the number of turns in its design which requires more energy to drive blood exhibiting high apparent viscosity, whereas the nature of the curve is linear in the case of STM. Close observation shows that with an increase in the mass loading of blood, the pressure drop increases but the mixing index reduces drastically in the case of STM and thus

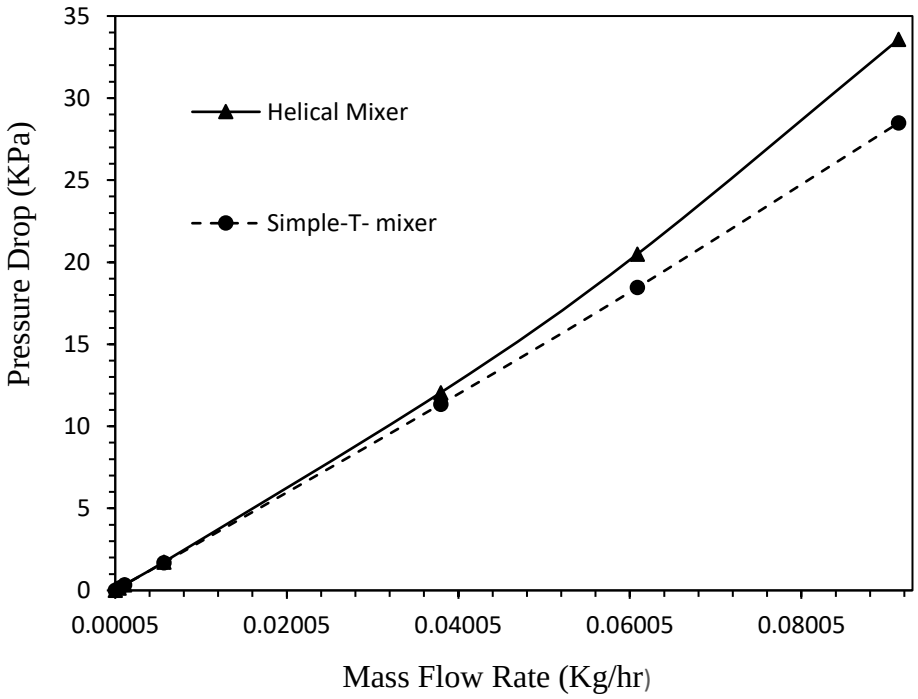

Figure 4.16 Variation of pressure drop with the mass flow rate for STM and TDHM with blood

4.3 Mixing and flow analysis of 3-dimensional helical micromixer (TDHM) possessing same axial length as that of STM

The results depicting the mixing performance with the same length of TDHM and STM were covered in-depth in the previous section of 4.2. This section thoroughly discusses the mixing performance of TDHM with the axial length of the mixer equal to the length of the conventional STM with a straight channel, i.e. 3000 µm. Although the axial length is assumed to be fixed for the micromixers, the mixing length or the peripheral length of TDHM is higher (~8810 µm) than STM due to the helical path of the channel introduced in the design. In the first part i.e. section 4.3.1, water (Newtonian fluid) is employed in the micromixer and results are presented for the flow behavior and the mixing index along with the comparison with the results of the conventional STM. Second section 4.3.2 examines the flow and mixing characteristics with the Non-Newtonian blood inside the micromixers.

4.3.1 TDHM (same axial length) with Newtonian fluid water as the working fluid

First, a comparison of mixing performance is presented between the STM and the TDHM based on the CFD visualization. Figure 4.17 (a) and (b) depicts the 3d streamlines based on the species concentration for STM and TDHM, respectively at Re=266.

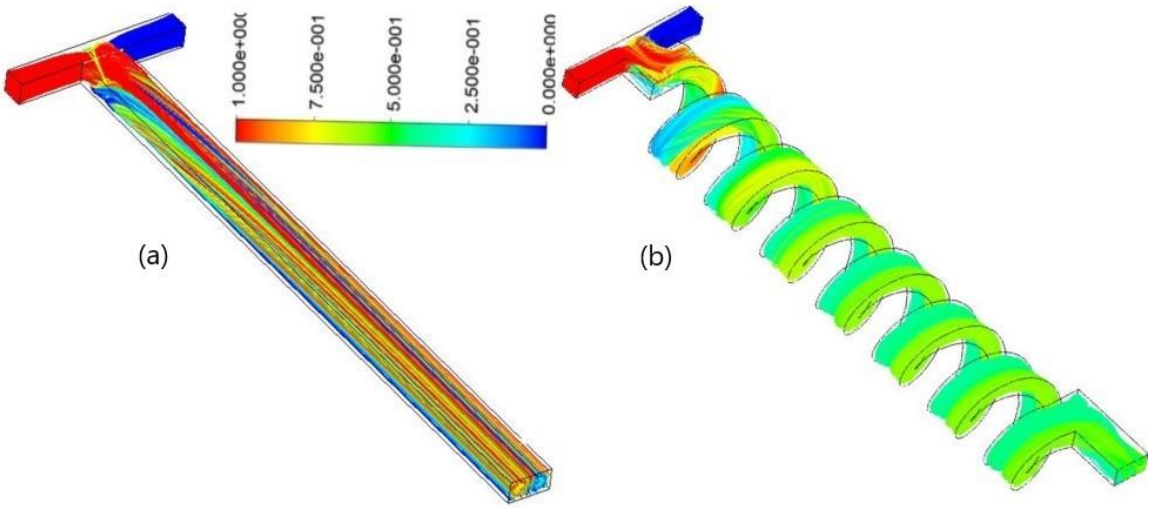

Figure4.17 Streamlines based on the species concentration for (a) STM and (b) TDHM at Re=266 (water)

It is inferred from the figure that higher mixing efficiency (87.8 %) is attained in the TDHM as compared to the STM with a mixing index of 30.7 % at the same Reynolds number of 266. Closer observation reveals that the complex 3-dimensional design of the mixing channel of TDHM produces significantly better mixing. The 3d curvature act as a twisting channel inducing the rotation in the fluid, furthermore this curvature introduces the centrifugal forces at the walls of the channel whose direction is changing with reversal of the channel in the opposite direction as the fluid travels in the axial direction towards the outlet leading to the enhancement in the mixing performance. The secondary flow enhances the mass diffusion and thus the mixing performance due to the creation of chaotic advection. Next, the discussion on the effect of Reynolds number on the mixing performance of the micromixer is examined.

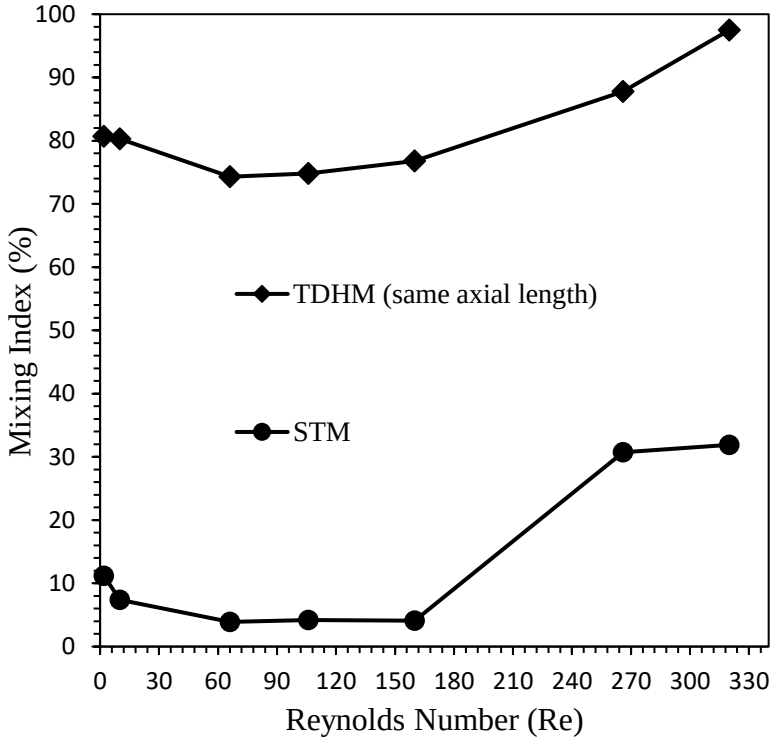

Figure 4.18 Variation of mixing index with Reynolds number

Figure 4.18 illustrates the variation of the mixing index with Reynolds for both STM and TDHM. It is obvious that at lower values of Reynolds number (Re≤10), the fluids have enough time to be in contact with mass diffusion to take place even though the flow falls in the laminar diffusion regime. Thus, a mixing index of 11.2 % for STM and 80.7 % for TDHM is obtained at Re=2. The basic reason for the higher mixing efficiency in TDHM is due to higher mixing length for the same axial distance and also more stretching&

folding of the flowing fluid due to the 3-dimensional twisting of the channel that enhances the area of contact of the two streams promoting the diffusion process. With an increase in Reynolds number, weak vortices are visible however a decreasing trend in the mixing index is noticed owing to the decrease in the residence time of fluids inside the mixing channels. This results in lesser time of contact of the two species and weak strength of vortices don't seem to have a significant impact on the mixing efficiency. The lowest value of the mixing index is 3.9 % for the conventional STM and 74.3 % for the proposed TDHM in this study, both at Re~66.

Here, the Vortex diffusion regime is observed until Re~ 160 for STM and Re~100 for TDHM after which the flow enters into the engulfment flow, and a sharp rise in the mixing performance is noted. Along with the engulfment flow, stronger secondary flow is visible in the TDHM due to the continuous rotation, twisting and stretching of the fluid layer that amplifies the mixing performance and complete mixing of fluid streams (97.5 %) is achieved at the maximum Reynolds number of 320 considered in the current investigation, whereas the maximum efficiency is 31.9 % for the straight channel STM. Figure 4.19 depicts the variation of the mixing index of TDHM with the axial distance (X) of the from the T-junction. Axial distance is the distance between the T-junction and the center of the plane taken for the calculation of the mixing performance, where X=0 µm represents the first plane as the fluid enters the helical channel after the T-junction.

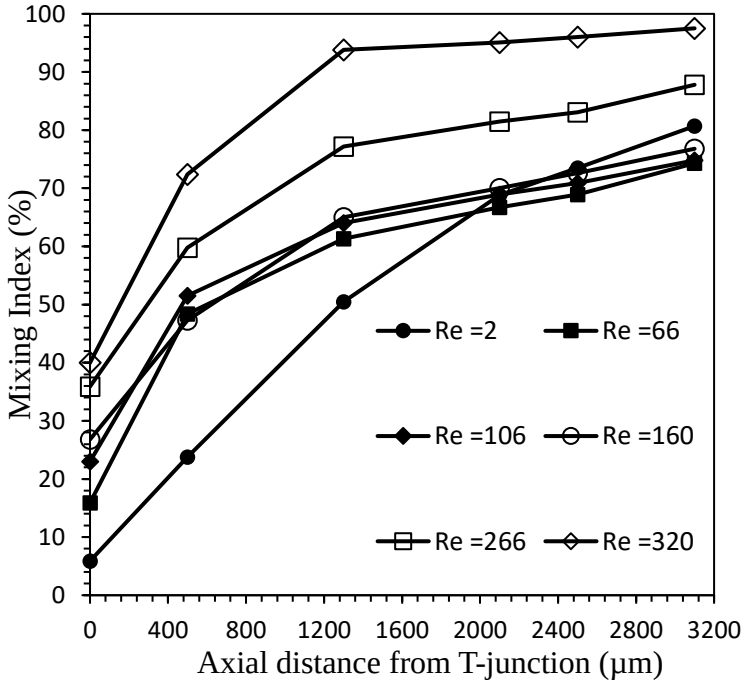

Figure 4.19 Variation of the mixing index with the axial distance at different values of Reynold number of water

The sharpest rise in the mixing performance from the inlet (5.89%) of the helical channel to the outlet (80.7 %) is seen for Re=2 due to the larger time available for the molecular diffusion to occur as discussed earlier. The slope of mixing index at different axial distances for Re~66, 106 & 160 appears to be almost the same. The mixing index for Re=320 rises from 40% to 97.5 % resulting in the complete mixing of the two streams. The variation of mixing index with axial distance from the inlet plane of the TDHM is shown in figure 4.20 for Re=266. The slope of the curve of STM appears to flatten after the axial length of 500 µm with a small increase in the efficiency from 25.1 % at 500 µm to 31.9 % at the outlet section of the conventional STM. At high Reynolds number as in this case, Re~266 the initial collision of the fluid streams at T-junction tend to provide a swirling motion to the fluids and penetrate into each other but owing to the straight channel in STM and lack of inertial forces in the flow field, there is an only mild increase in the mixing efficiency after 500 µm. Whereas, a continuous rise is observed from 35.9 % on the inlet section of TDHM to 87.8% at the outlet section because of the stronger strength of secondary motion. Therefore, the TDHM is a better choice over STM to gain effective mixing within a short axial distance for both low and high Reynolds number flow.

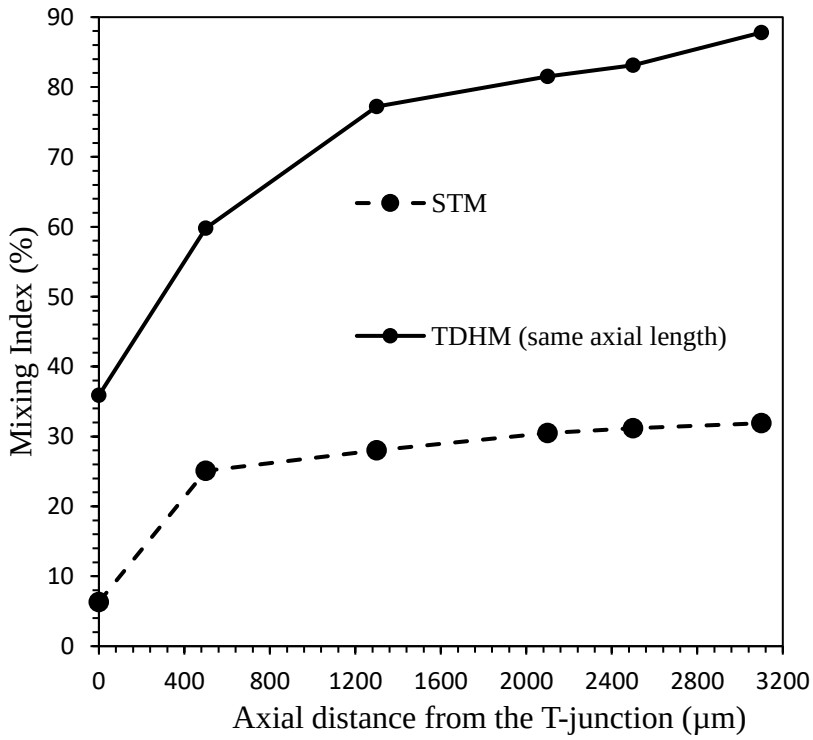

Figure 4.20 Comparison of mixing index of STM and TDHM at various cross-sections along with different axial distances for Re=266.

To visualize the amount of mixing achieved at different planes considered at different axial distances from the inlet, contours of species concentration at different planes for five different Reynolds numbers that are 2,66, 106, 160 & 320 is shown in figure 14.21. At Re=2, the interface between the mixing fluid appears narrow and thin on initial planes informing about the laminar diffusion regime with no signs of vortices or secondary flow. Still, good mixing is achieved at the outlet because of the stretching of the fluid interface and the high time of contact of the fluids inside the microchannels as seen in the successive sections of Re=2. For Re= 66, 106 & 160, the interfacial area increases as the flow progresses to further planes in the channel due to the weak vortices which are introduced with an increase of the Reynolds number. At Re=320, the inertia of the fluid supports the rotation of the fluid streams, and the strong secondary motion results in the complete mixing of the streams at the outlet section.

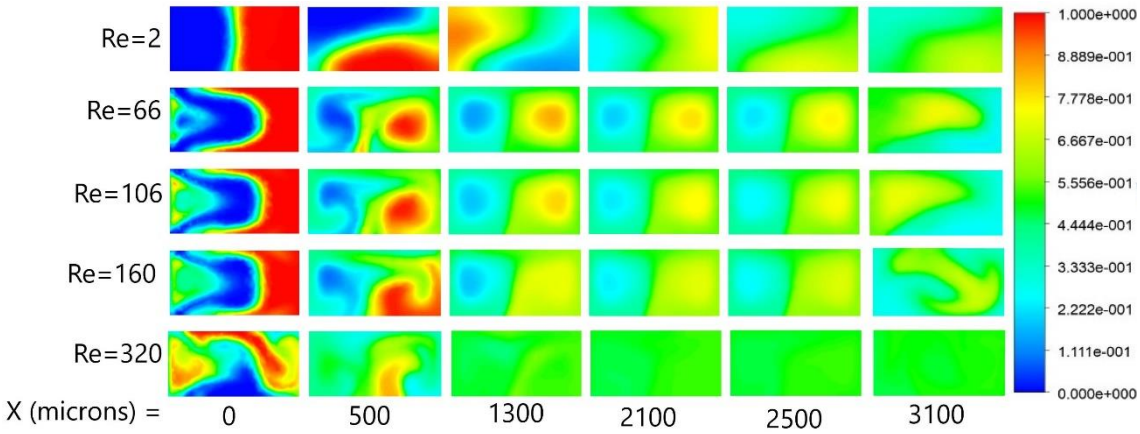

Figure 4.21 Species concentration distribution of water in TDHM at different sections considered along the length of the microchannel.

Pressure drop is a crucial parameter to understand the power requirements to drive the fluids inside the micromixer. Figure 4.22 shows the effect of Reynolds number on the pressure drop that occurs between the inlets and outlet of the TDHM. It is visible that with Reynolds number the pressure drop increases rapidly. At the lowest value of Reynolds number considered in the study, i.e. 2 the pressure drop is 0.278 KPa whereas it is 1.40 KPa at Re=10. This increasing trend is observed throughout the wide range of Reynolds number with a maximum pressure drop 95.183 KPa calculated at the maximum value of Reynolds number, i.e. 320. Since the mixing lengths of the STM and TDHM is different in this case, it is not feasible to make a comparison between the pressure drops of the two micromixers. Moreover, a brief study on the pressure drops of STM and TDHM

possessing the same peripheral length of 3000 microns and having water as the working fluid is presented earlier in section 4.2.1 and can be referred to.

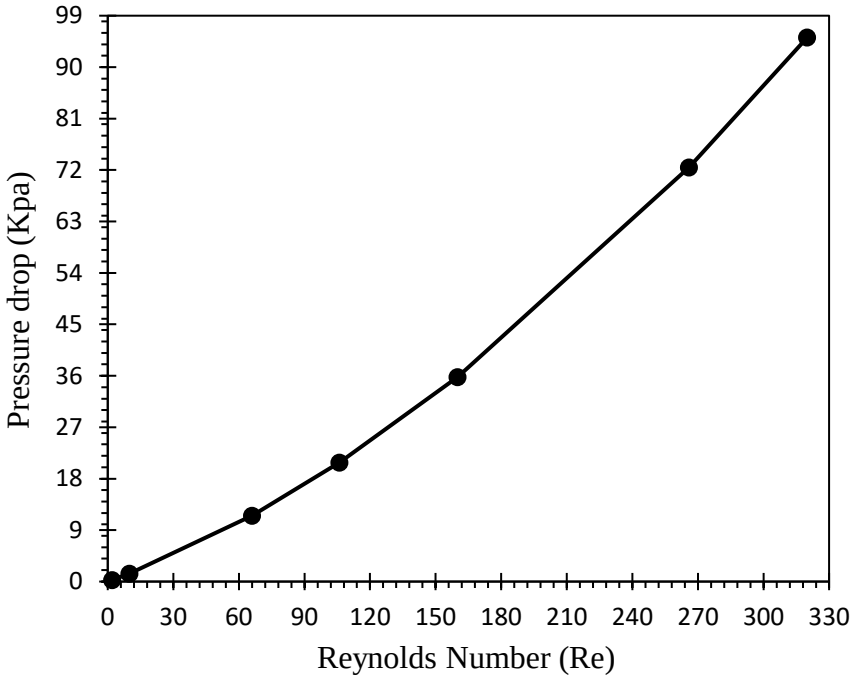

Figure 4.22 Pressure drop variation in TDHM (same axial length) with Reynolds number.

4.3.2 TDHM (same axial length) with Non-Newtonian blood as the working fluid

As discussed previously in section 3.3.1, the Carreau-Yasuda is used to numerically model the shear thinning characteristics of blood (Non-Newtonian). Although at small values of mass loading, blood behaves as a Newtonian fluid as seen in figure 3.5, the apparent viscosity of blood is approximately 150 times the viscosity of water at a strain rate of 0.00001 s^{-1}. A continuous drop is seen in the apparent viscosity of blood with an increase in the strain rate with viscosity eventually becoming asymptotic having a value of 0.00350 Pa-s. However, the apparent viscosity of blood is still 3.5 times higher than the viscosity of water, i.e. 0.001 Pa-s. This wide variation of apparent viscosities over an extensive range of strain rate causes it to exhibit different mixing performance and flow characteristics relative to the water which is a Newtonian fluid.

Figure 4.23 (a) & (b) shows the streamlines based on the mass fraction of the mixing species for straight channel STM and proposed TDHM respectively at the lowest value of mass flow rate of blood (~0.00005 Kg/hr) considered in the current investigation. It is clearly visible that higher diffusion of species takes in the case of TDHM on account of

the longer mixing length availability in TDHM providing sufficient time to mass diffusion to occur that is the sole mechanism of mass transport and thus mixing at such a low-value of mass loading.

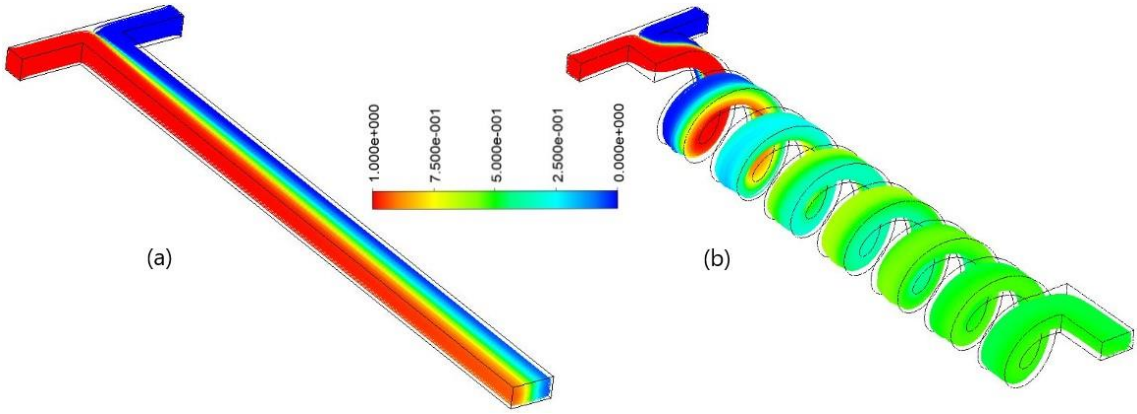

Figure 4.23 Streamlines based on the mass fraction concentrations of the mixing fluid, i.e. blood at ṁ =0.00005 kg/hr for (a) STM & (b) TDHM (same axial length)

The mixing efficiency or index attained by STM at the outlet is 34.5 % while it is 97 % for STM. The fluid streams appear to flow smoothly through the microchannel without any indication of the formation of vortices at low mass flow rates. As the mass flow rate is increased the fluid streams exit the mixer at a faster rate which results in the reduction of the mixing as seen in figure 4.24 which depicts the streamlines based on the mass fraction distribution in the flow domain for ṁ = 0.00143 kg/hr. Although a drop is observed in mixing performance with an increase in the mass flow rate for both the micromixer, Still the TDHM produce superior results (50.4 %) over the STM (6.01%) within a shorter axial distance that can be visualized in figure 4.24 (a) & (b).

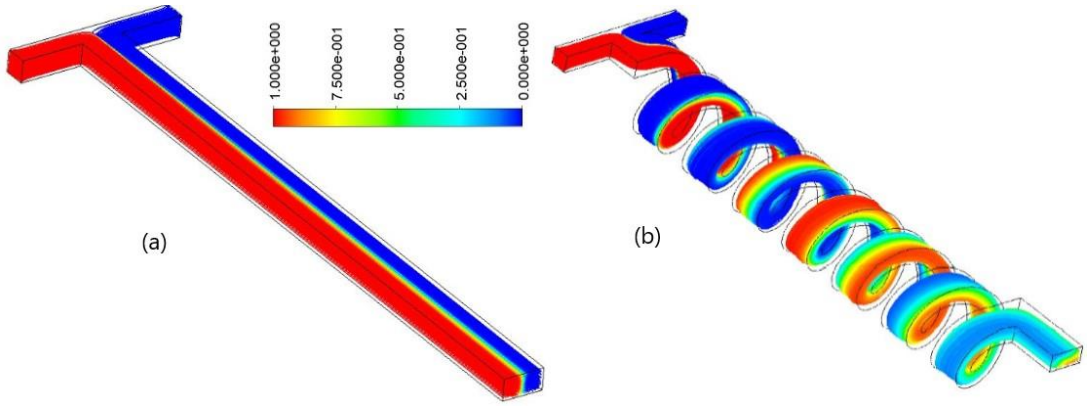

Figure 4.24 Streamlines based on the mass fraction concentrations of the mixing fluid, i.e. blood at ṁ =0.00143 kg/hr for (a) STM & (b) TDHM (same axial length).

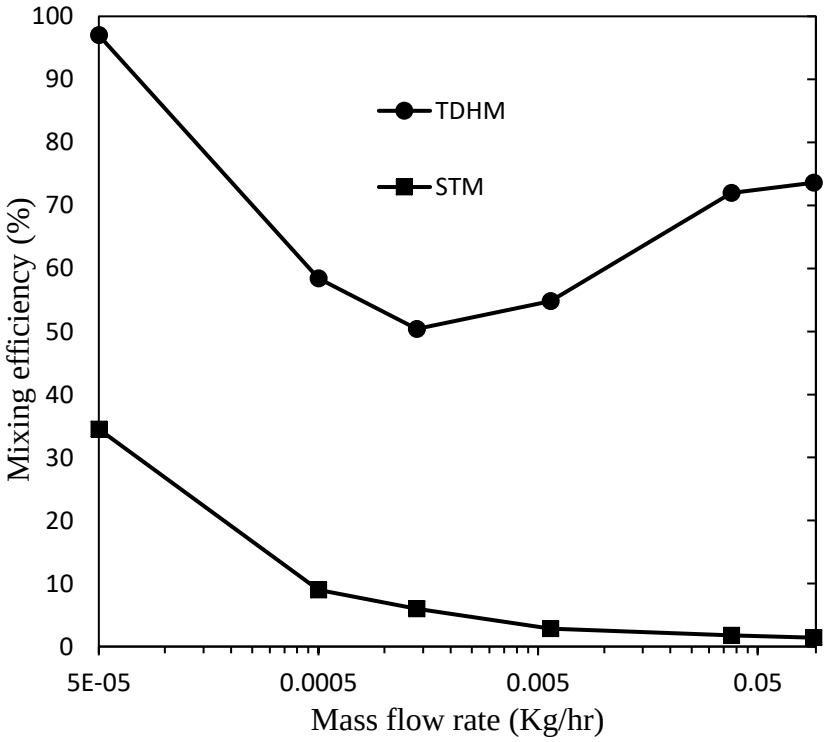

Figure 4.25 Variation of mixing efficiency with the mass flow rate of blood for STM and TDHM (same axial length)

Figure 4.25 shows the effect of the mass flow rate of blood on the mixing efficiency for both STM and TDHM for a wide range of flow rates. A continuous decreasing trend is visible for the mixing efficiency in the case of conventional STM whereas a decreasing pattern is by the mixing efficiency curve of TDHM. It is understood from a discussion on the conventional STM that highly viscous blood doesn't support the swirling motion or the secondary flow even at high values of mass loading due to the presence of strong magnitude viscous forces and hence no engulfment zone is seen even at high mass flow rates. This hampers the mixing performance in STM leading to poor mixing quality at higher mass loading values with minimum reaching to as low as 1.41 % at the highest mass flow rate of 0.09 Kg/hr. The maximum mixing achieved in STM is 34.5 % at the lowest mass flow due to the higher available time for diffusion. On the other hand, the mixing performance of TDHM is seen as superior at all the values of the mass flow rate. Complete mixing of streams (97 %) is gained at the lowest mass flow rate (0.00005 Kg/hr) considered in the study. The mixing performance decreases significantly until the mass flow of 0.0014 Kg/hr, after which the magnitude of centrifugal forces rises that pushes the mixing streams towards the outer wall of the helical channel resulting in an intensification of the secondary flow. This leads to stretching, folding, and rotation of the

fluid at a faster rate, and thus enhancement in the mixing efficiency is visible. The mixing index rises sharply from 50.4 % at 0.00143 Kg/hr to 73.6 % at 0.09 Kg/hr indication the benefit of employing the proposed TDHM for mixing shear-thinning fluids like blood at both high and low mass loadings. Figure 4.26 illustrates the mixing index in the TDHM at various successive planes along the axial direction of the flow for a various mass flow rates of blood.

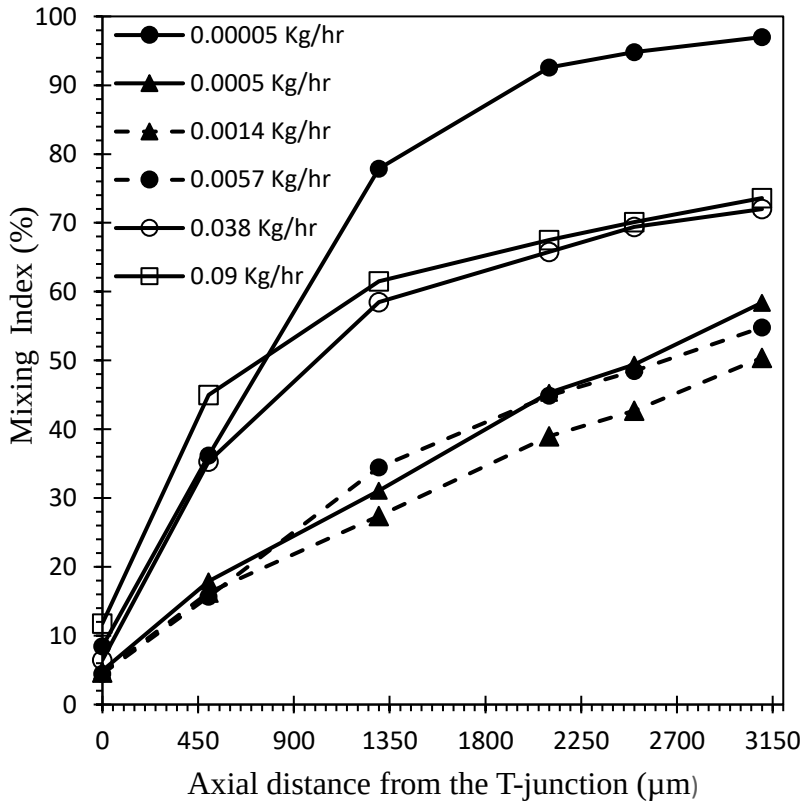

Figure 4.26 Variation of the mixing index with the axial distance at different values of mass flow rates of blood

It is inferred from the figure that the steepest rise in mixing index from entry to the exit of the micromixer is for the lowest mass flow rate of blood (0.00005 Kg/hr) with an increase from 8.46 % to 97 % giving complete mixing. The variation of mixing index curves calculated at $\dot{m}$ = 0.0005 Kg/hr, 0.00143 kg/hr, and 0.0057 Kg/hr can be approximated to linear behavior with the axial distance of the mixer and also the mixing efficiency remains almost equal for the axial distance less than 500 µm while a close observation reveals a small variation is present on planes thereafter. With a further increase in the mass flow rate to 0.038 Kg/hr and 0.09 Kg/hr, the slope of the mixing curve rises rapidly till X=500 µm, while after that the mixing index rises slowly on the successive planes with highest reaching to 73.6 % at the outlet. Visualization of the

amount of mixing that takes place at different planes located at several distinct locations from the T-

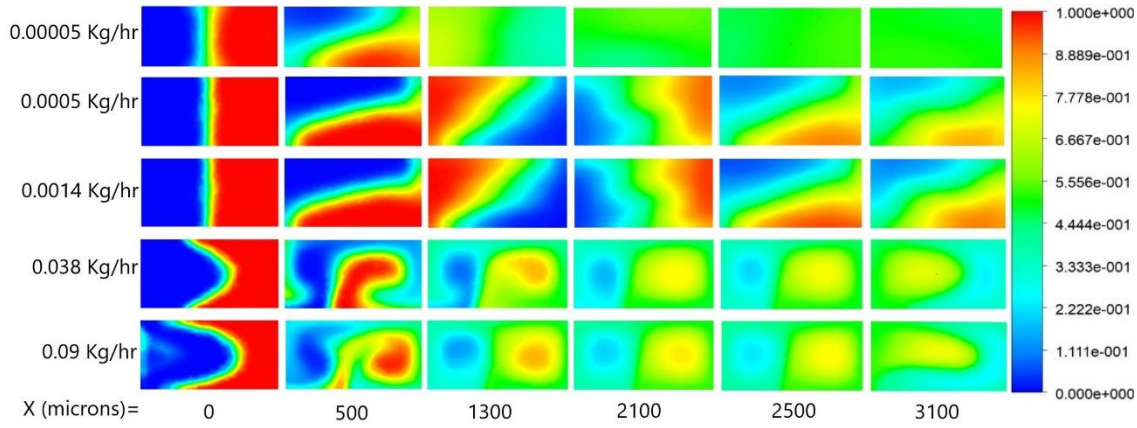

Figure 4.27 Species concentration distribution of water in TDHM at different sections considered along the length of the microchannel

junctions are shown in figure 4.27. It depicts the concentration of mass fraction of species to obtain a clear idea of the interface interaction and mixing mechanism. For $\dot{m}$ =0.00005 kg/hr, the interface between the fluid streams looks straight at the entrance of the helical microchannel and becomes diagonal at a location of 500 microns with a growth in the thickness of the diffusion zone leading to increase in the mixing index. Since the mass flow rate is low, completely mixed fluid is obtained at the outlet of micromixer (refer to the first row of figures). With an increase in the mass flow rate (0.0005 Kg/hr & 0.0014 Kg/hr), the interface shrinks in size and is symmetrical at the entrance plane. This results in a significant drop in the mixing performance and lower mixed fluids are obtained at the outlet section. Increasing mass loading to 0.038 Kg/hr, the symmetry of the fluid interface is broken at the inlet plane causing an enhancement in the interfacial area that boosts the mass diffusion transport mechanism. The secondary flow promotes advancement in the mixing mechanism and therefore we observe a boost in the mixing performance with an increase of the mass flow rates of blood after $\dot{m}$ =0.0014 Kg/hr.

Figure 4.28 presents the variation of pressure drop inside the 3-dimensional helical microchannel with the mass rate of blood. The pressure drop increases promptly with an increase in the mass flow rates. The maximum pressure drops of 90.32 KPa is obtained at the highest flow rate in the study, i.e. $\dot{m}$ =0.09 Kg/hr and it is concluded that the improvement in mixing performance always comes with more energy requirements to drive the flow.

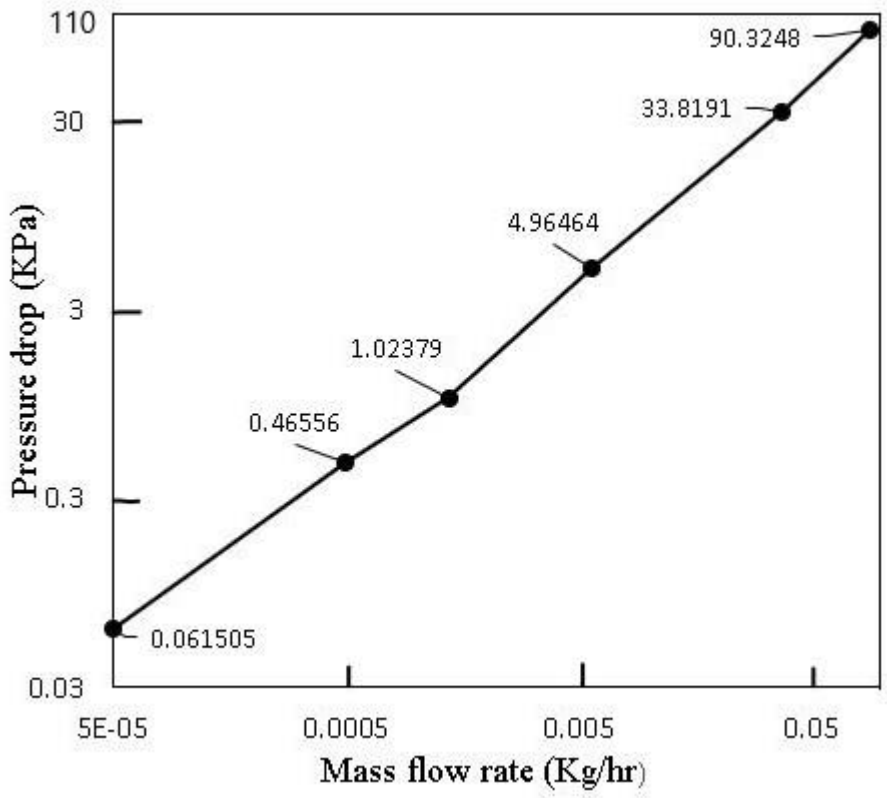

Figure 4.28 Pressure drop variation in TDHM (same axial length) with the mass flow rate of blood.

4.4 A Comparison of mixing and pressure drop in TDHM between Newtonian and Non-Newtonian fluid

The two fluids considered in the study are blood and water that exhibit different rheological characteristics which makes it important to examine how the mixing performance is changing with the change of the fluid and also the investigation of energy requirements for the fluid transport is done with the help of comparison of pressure drop that occurs in TDHM between inlets and outlet for both Newtonian and Non-Newtonian fluid. It is understood that the viscosity of water remains constant (0.001 Pa-s) with an increase or decrease in the shear rate as it is a Newtonian fluid whereas the apparent viscosity of blood higher as compared to water and changes with variation in the shear strain rate. Figure 4.29 shows the variation of mixing index in for water in the range of 2~160 Reynolds number and for blood with the corresponding range of blood mass flow rate starting from 0.0014 Kg/hr up to 0.091 Kg/hr. It is observed from the figure that mixing is superior for water at all the values of the mass flow rate when compared to the mixing performance of water.

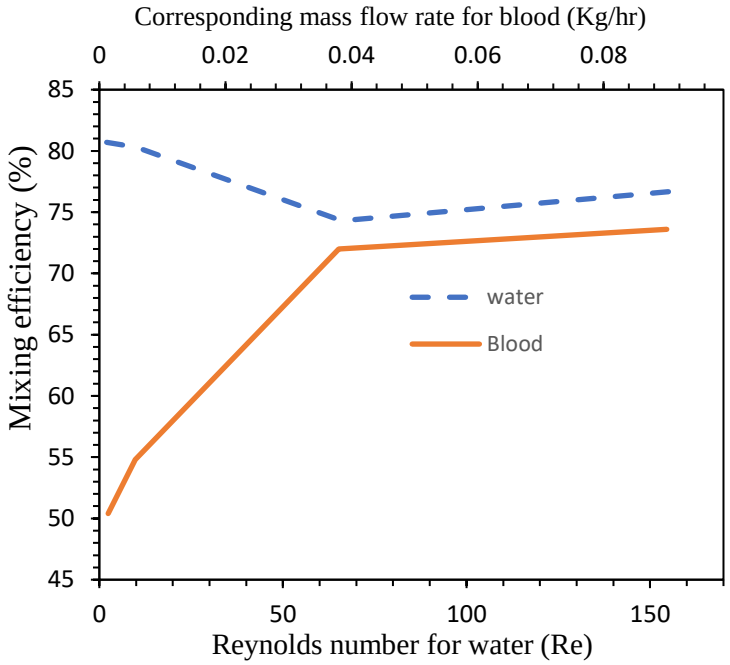

Figure 4.29 Comparison of mixing efficiency for Newtonian and Non-Newtonian fluid in TDHM

At Re=2, there exist a significant difference (30.3 %) between the mixing efficiencies of blood and water. However, with an increase in the Reynolds number the mixing efficiency curves seem to approach each other and a small difference of 2.3% is noticed at Re= 66. The better mixing performance witnessed for water can be accounted to its lower viscosity as more inertia of fluid helps in the development of stronger secondary flow in the case of water, whereas high viscosity of blood opposes the formation of vortices and try to dampen its effects. This is also the reason behind the absence of engulfment flow regime for blood in the conventional STM making it a bad choice while dealing with blood and therefore TDHM stand out to be a better pick.

Figure 4.30 shows the comparison of pressure drop in TDHM between water (Newtonian) and blood (Non-Newtonian) for a wide range of Reynolds number, i.e. $2 \leq Re \leq 160$ and the corresponding range of the mass flow rate of the blood. The higher viscosity of blood results in the higher magnitude of the viscous forces in the blood which offers larger resistance to the flow when compared to the water and hence, the energy requirements increase drastically with an increase in the mass flow rate for blood. At Re=2, the pressure drop in the case of blood is 3.68 times relative to the pressure drop obtained for water. The pressure drop rises for blood sharp whereas it is gradual for water. The pressure drops incurred at Re=160 are 90.23 KPa compared to 35.803 KPa for water and it is clear from

all the calculations that more power is required to drive the blood through the helical microchannel.

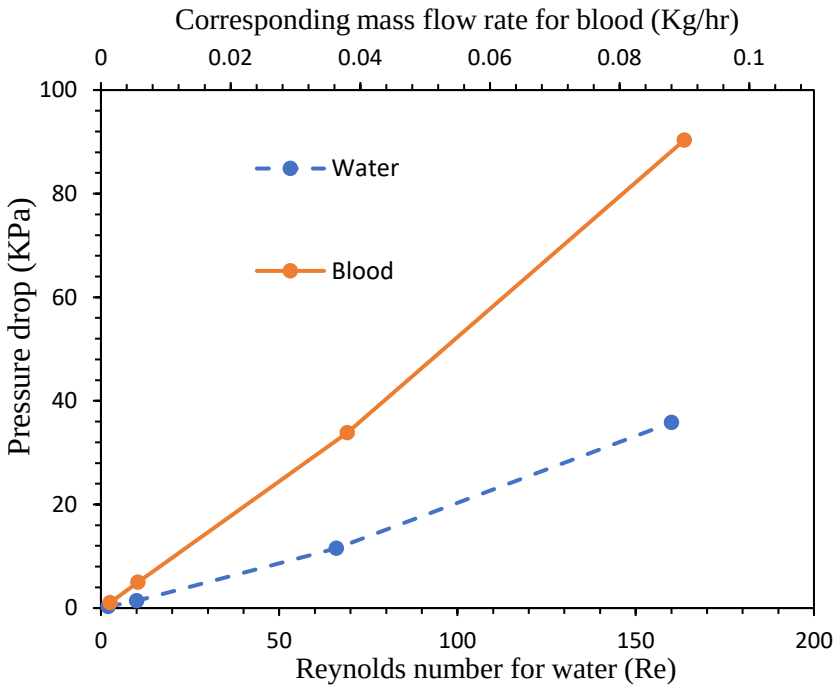

Figure 4.30 Comparison of pressure drop incurred in TDHM for blood and water

CHAPTER 5

THESIS CONCLUSION

Mixing performances of a basic T-micromixer (STM) & a novel 3-dimensional helical passive micromixer (TDHM) having rectangular cross-section were investigated for Newtonian fluid water and Non-Newtonian fluid blood with the help of CFD simulations and a brief discussion highlighted the distinctive nature of blood compared to the Newtonian fluid water considered in the analysis. At lower values of Reynolds number (Re=2) and the corresponding mass flow rate of blood (0.00005 kg/hr), better mixing is achieved in the case of TDHM due to the increase in the interfacial area between the two mixing streams and a notable improvement in mixing index of 40.5 % was obtained in the case of a Newtonian fluid, whereas the increase, was 34.3 % for Non-Newtonian fluid. STM performs poorly at high mass flow rates (≥ 0.0005 Kg/hr) of Non-Newtonian fluid (Carreau-Yasuda model) whereas TDHM achieves good mixing at high mass flow rate due to the formation of secondary flow creating the chaotic advection with a remarkable difference of 53.49 % in the mixing index contrary to the STM. Another great advantage of TDHM is that it reduces the total axial distance required to gain efficient mixing for both Newtonian and Non-Newtonian fluid. Although the peripheral length taken is the same as that of the STM (3 mm), however, the total axial length of the TDHM was 0.741 mm, making it an efficient micromixer for practical applications.

Another study is performed fixing the axial length of STM and TDHM to be 3000 microns. The fluids mixed completely (97.5%) at high Reynolds number in the case of a Newtonian fluid whereas the efficiency obtained at the maximum mass flow rate of blood is 73.6%. Also, a comparative study is presented in the form of graphs, streamlines, and concentration contours of fluids at different planes between the Newtonian and Non-Newtonian fluids to understand the variation of mixing performance with the change of the working fluid inside the microchannels.

Furthermore, a deep analysis of the pressure drop that occurs between the inlets and outlet of the micromixer is done for all the micromixers in the study. It is found that more pressure drop occurs when the working fluid exhibits Non-Newtonian characteristics and thus more power is required to mix the blood in microchannels as compared to water which exhibits Newtonian characteristics and has lesser viscosity.

5.1 Scope of future work

Future work can involve investigating the effect of various geometrical parameters like the cross-sectional area, pitch length, mean diameter of the helical curve, etc on the mixing index and finally optimizing the micromixer from the collected data to obtain the best mixing performance in the helical channels.

Furthermore, some periodic obstructions can be introduced in the path of the flowing fluids to create disturbances which will further enhance the chaotic advection and analysis can be performed to find the optimum option for maximum mixing with a minimum pressure drop.

REFERENCES

[1] G. Cai, L. Xue, H. Zhang, and J. Lin, "A review on micromixers," *Micromachines*, vol. 8, no. 9, 2017, doi: 10.3390/mi8090274.

[2] R. Article, P. Eribol, and A. K. Uguz, "Experimental investigation of electrohydrodynamic instabilities in micro channels," vol. m, pp. 425–434, 2015, doi: 10.1140/epjst/e2015-02371-5.

[3] C. A. Cortes-quiroz, A. Azarbadegan, I. D. Johnston, and M. C. Tracey, "Analysis and design optimization of an integrated micropump-micromixer operated for bio-MEMS applications," vol. 1, no. September, pp. 7–10, 2014.

[4] K. Khoshmanesh, A. Almansouri, H. Albloushi, P. Yi, and R. Soffe, "A multi-functional bubble-based microfluidic system," 2015, doi: 10.1038/srep09942.

[5] S. Qian and H. H. Bau, "Magneto-hydrodynamic stirrer for stationary and moving fluids," vol. 106, no. July 2004, pp. 859–870, 2005, doi: 10.1016/j.snb.2004.07.011.

[6] N. Veldurthi, S. Chandel, T. Bhave, and D. Bodas, "Sensors and Actuators B : Chemical Computational fluid dynamic analysis of poly (dimethyl siloxane) magnetic actuator based micromixer," *Sensors Actuators B. Chem.*, vol. 212, pp. 419–424, 2015, doi: 10.1016/j.snb.2015.02.048.

[7] B. S. Haeberle, T. Brenner, H. Schlosser, R. Zengerle, and J. Ducrøe, "Centrifugal Micromixer," no. 5, pp. 613–616, 2005, doi: 10.1002/ceat.200407138.

[8] G. S. Jeong, S. Chung, C. B. Kim, and S. H. Lee, "Applications of micromixing technology," *Analyst*, vol. 135, no. 3, pp. 460–473, 2010, doi: 10.1039/b921430e.

[9] N. T. Nguyen and Z. Wu, "Micromixers - A review," *J. Micromechanics Microengineering*, vol. 15, no. 2, 2005, doi: 10.1088/0960-1317/15/2/R01.

[10] W. Raza, S. Hossain, and K.-Y. Kim, "A Review of Passive Micromixers with a Comparative Analysis," *Micromachines*, vol. 11, no. 5, p. 455, 2020, doi: 10.3390/mi11050455.

[11] V. Hessel, H. Löwe, and F. Schönfeld, "Micromixers - A review on passive and active mixing principles," *Chem. Eng. Sci.*, vol. 60, no. 8-9 SPEC. ISS., pp. 2479–

2501, 2005, doi: 10.1016/j.ces.2004.11.033.

[12] M. Bayareh, M. N. Ashani, and A. Usefian, “Active and passive micromixers: A comprehensive review,” *Chem. Eng. Process. - Process Intensif.*, vol. 147, p. 107771, 2020, doi: 10.1016/j.cep.2019.107771.

[13] H. Search, C. Journals, A. Contact, M. Iopscience, and I. P. Address, “Two simple micromixers based on silicon,” vol. 123, pp. 5–9.

[14] H. Search, C. Journals, A. Contact, M. Iopscience, and I. P. Address, “Characterization method for a new diffusion mixer applicable in micro flow injection analysis systems,” vol. 199, pp. 2–6, 1999.

[15] D. Gobby, P. Angeli, and A. Gavriilidis, “Mixing characteristics of T-type microfluidic mixers,” vol. 126, 2001.

[16] D. Bothe, C. Stemich, and H. J. Warnecke, “Fluid mixing in a T-shaped micro-mixer,” *Chem. Eng. Sci.*, vol. 61, no. 9, pp. 2950–2958, 2006, doi: 10.1016/j.ces.2005.10.060.

[17] S. H. Wong, M. C. L. Ward, and C. W. Wharton, “Micro T-mixer as a rapid mixing micromixer,” *Sensors Actuators, B Chem.*, vol. 100, no. 3, pp. 359–379, 2004, doi: 10.1016/j.snb.2004.02.008.

[18] A. Soleymani, E. Kolehmainen, and I. Turunen, “Numerical and experimental investigations of liquid mixing in T-type micromixers,” *Chem. Eng. J.*, vol. 135, no. SUPPL. 1, 2008, doi: 10.1016/j.cej.2007.07.048.

[19] T. Andreussi, C. Galletti, R. Mauri, S. Camarri, and M. V. Salvetti, “Flow regimes in T-shaped micro-mixers,” *Comput. Chem. Eng.*, vol. 76, pp. 150–159, 2015, doi: 10.1016/j.compchemeng.2015.02.017.

[20] T. Matsunaga, H. J. Lee, and K. Nishino, “An approach for accurate simulation of liquid mixing in a T-shaped micromixer,” *Lab Chip*, vol. 13, no. 8, pp. 1515–1521, 2013, doi: 10.1039/c3lc41009a.

[21] M. A. Ansari, K. Y. Kim, and S. M. Kim, “Numerical study of the effect on mixing of the position of fluid stream interfaces in a rectangular microchannel,” *Microsyst. Technol.*, vol. 16, no. 10, pp. 1757–1763, 2010, doi: 10.1007/s00542-010-1100-2.

[22] A. S. Lobasov, A. V. Minakov, V. V. Kuznetsov, V. Y. Rudyak, and A. A. Shebeleva, “Investigation of mixing efficiency and pressure drop in T-shaped micromixers,” *Chem. Eng. Process. - Process Intensif.*, vol. 134, pp. 105–114, 2018, doi: 10.1016/j.cep.2018.10.012.

[23] C. A. Cortes-Quiroz, A. Azarbadegan, and M. Zangeneh, “Evaluation of flow characteristics that give higher mixing performance in the 3-D T-mixer versus the typical T-mixer,” *Sensors Actuators, B Chem.*, vol. 202, pp. 1209–1219, 2014, doi: 10.1016/j.snb.2014.06.042.

[24] S. Sarkar, K. K. Singh, V. Shankar, and K. T. Shenoy, “CFD simulations to study the effects of wall protrusions on microfluidic mixing,” *J. Micromechanics Microengineering*, vol. 25, no. 8, p. 84008, 2015, doi: 10.1088/0960-1317/25/8/084008.

[25] T. M. Dundi, V. R. K. Raju, and V. P. Chandramohan, “Numerical evaluation of swirl effect on liquid mixing in a passive T-micromixer,” *Aust. J. Mech. Eng.*, vol. 00, no. 00, pp. 1–15, 2019, doi: 10.1080/14484846.2019.1626527.

[26] A. A. S. Bhagat, E. T. K. Peterson, and I. Papautsky, “A passive planar micromixer with obstructions for mixing at low Reynolds numbers,” *J. Micromechanics Microengineering*, vol. 17, no. 5, pp. 1017–1024, 2007, doi: 10.1088/0960-1317/17/5/023.

[27] N. Ait Mouheb, D. Malsch, A. Montillet, C. Solliec, and T. Henkel, “Numerical and experimental investigations of mixing in T-shaped and cross-shaped micromixers,” *Chem. Eng. Sci.*, vol. 68, no. 1, pp. 278–289, 2012, doi: 10.1016/j.ces.2011.09.036.

[28] M. Kashid, A. Renken, and L. Kiwi-Minsker, “Mixing efficiency and energy consumption for five generic microchannel designs,” *Chem. Eng. J.*, vol. 167, no. 2–3, pp. 436–443, 2011, doi: 10.1016/j.cej.2010.09.078.

[29] S. Hossain and K.-Y. Kim, “Numerical Study on Mixing Performance of Straight Groove Micromixers,” *Int. J. Fluid Mach. Syst.*, vol. 3, no. 3, pp. 227–234, 2010, doi: 10.5293/ijfms.2010.3.3.227.

[30] S. Sarkar, K. K. Singh, V. Shankar, and K. T. Shenoy, “Numerical simulation of mixing at 1-1 and 1-2 microfluidic junctions,” *Chem. Eng. Process. Process Intensif.*, vol. 85, pp. 227–240, 2014, doi: 10.1016/j.cep.2014.08.010.

[31] S. Hossain, M. A. Ansari, and K. Y. Kim, “Evaluation of the mixing performance of three passive micromixers,” *Chem. Eng. J.*, vol. 150, no. 2–3, pp. 492–501, 2009, doi: 10.1016/j.cej.2009.02.033.

[32] A. Afzal and K. Y. Kim, “Mixing performance of passive micromixer with sinusoidal channel walls,” *J. Chem. Eng. Japan*, vol. 46, no. 3, pp. 230–238, 2013,

doi: 10.1252/jcej.12we144.

[33] S. Rampalli, T. M. Dundi, S. Chandrasekhar, V. R. K. Raju, and V. P. Chandramohan, "Numerical Evaluation of Liquid Mixing in a Serpentine Square Convergent-divergent Passive Micromixer," *Chem. Prod. Process Model.*, pp. 1–11, 2020, doi: 10.1515/cppm-2019-0071.

[34] L. Balasubramaniam, R. Arayanarakool, S. D. Marshall, B. Li, P. S. Lee, and P. C. Y. Chen, "Impact of cross-sectional geometry on mixing performance of spiral microfluidic channels characterized by swirling strength of Dean-vortices," *J. Micromechanics Microengineering*, vol. 27, no. 9, 2017, doi: 10.1088/1361-6439/aa7fc8.

[35] M. Rafeie, M. Welleweerd, A. Hassanzadeh-Barforoushi, M. Asadnia, W. Olthuis, and M. E. Warkiani, "An easily fabricated three-dimensional threaded lemniscate-shaped micromixer for a wide range of flow rates," *Biomicrofluidics*, vol. 11, no. 1, 2017, doi: 10.1063/1.4974904.

[36] J. Yang, L. Qi, Y. Chen, and H. Ma, "Design and fabrication of a three dimensional spiral micromixer," *Chinese J. Chem.*, vol. 31, no. 2, pp. 209–214, 2013, doi: 10.1002/cjoc.201200922.

[37] K. Liu *et al.*, "A high-efficiency three-dimensional helical micromixer in fused silica," *Microsyst. Technol.*, vol. 19, no. 7, pp. 1033–1040, 2013, doi: 10.1007/s00542-012-1695-6.

[38] D. Tachibana *et al.*, "3D Helical Micromixer Fabricated by Micro Lost-Wax Casting," *Adv. Mater. Technol.*, vol. 5, no. 1, pp. 1–7, 2020, doi: 10.1002/admt.201900794.

[39] C. Shan, F. Chen, Q. Yang, Z. Jiang, and X. Hou, "3D multi-microchannel helical mixer fabricated by femtosecond laser inside fused silica," *Micromachines*, vol. 9, no. 1, pp. 1–7, 2018, doi: 10.3390/mi9010029.

[40] S. Baheri Islami, M. Khezerloo, and R. Gharraei, "The effect of chaotic advection on mixing degree and pressure drop of non-Newtonian fluids flow in curved micromixers," *J. Brazilian Soc. Mech. Sci. Eng.*, vol. 39, no. 3, pp. 813–831, 2017, doi: 10.1007/s40430-016-0689-1.

[41] S. Baheri Islami and M. Khezerloo, "Enhancement of mixing performance of non-newtonian fluids using curving and grooving of microchannels," *J. Appl. Fluid Mech.*, vol. 10, no. 1, pp. 127–141, 2017, doi:

10.18869/acadpub.jafm.73.238.26374.

[42] Z. Qiao, Z. Wang, C. Zhang, S. Yuan, Y. Zhu, and J. Wang, “PVAm–PIP/PS composite membrane with high performance for CO_2/N_2 separation,” *AIChE J.*, vol. 59, no. 4, pp. 215–228, 2012, doi: 10.1002/aic.

[43] A. Afzal and K. Y. Kim, *Flow and mixing analysis of non-Newtonian fluids in straight and serpentine microchannels*, vol. 116. Elsevier, 2014.

[44] A. Husain, N. Z. Al-Rawahi, F. A. Khan, and A. Samad, “Blood flow and mixing analysis in split-and-recombine micromixer with offset fluid inlets,” *Am. Soc. Mech. Eng. Fluids Eng. Div. FEDSM*, vol. 3, pp. 1–5, 2018, doi: 10.1115/FEDSM2018-83468.

[45] J. N. Kuo, H. S. Liao, and X. M. Li, “Design optimization of capillary-driven micromixer with square-wave microchannel for blood plasma mixing,” *Microsyst. Technol.*, vol. 23, no. 3, pp. 721–730, 2017, doi: 10.1007/s00542-015-2722-1.

[46] J. Boyd, J. M. Buick, and S. Green, “Analysis of the Casson and Carreau-Yasuda non-Newtonian blood models in steady and oscillatory flows using the lattice Boltzmann method,” *Phys. Fluids*, vol. 19, no. 9, 2007, doi: 10.1063/1.2772250.

[47] F. Abraham, M. Behr, and M. Heinkenschloss, “Shape optimization in steady blood flow: A numerical study of non-Newtonian effects,” *Comput. Methods Biomech. Biomed. Engin.*, vol. 8, no. 2, pp. 127–137, 2005, doi: 10.1080/10255840500180799.

[48] S. Koksungnoen, P. Rattanadecho, and P. Wongchadakul, “3D numerical model of blood flow in the coronary artery bypass graft during no pulse and pulse situations: Effects of an anastomotic angle and characteristics of fluid,” *J. Mech. Sci. Technol.*, vol. 32, no. 9, pp. 4545–4552, 2018, doi: 10.1007/s12206-018-0851-z.

[49] S. Tabakova, E. Nikolova, and S. Radev, “Carreau model for oscillatory blood flow in a tube,” *AIP Conf. Proc.*, vol. 1629, no. February, pp. 336–343, 2014, doi: 10.1063/1.4902290.

[50] A. Afzal and K. Y. Kim, *Flow and mixing analysis of non-Newtonian fluids in straight and serpentine microchannels*, vol. 116. Elsevier, 2014.

[51] J. Hussong, R. Lindken, M. Pourquie, and J. Westerweel, “Numerical study on the flow physics of a T-shaped micro mixer,” *IUTAM Bookseries*, vol. 15, pp. 191–205, 2009, doi: 10.1007/978-90-481-2626-2_15.

[52] A. P. Sudarsan and V. M. Ugaz, “Fluid mixing in planar spiral microchannels,” *R. Soc. Chem.*, pp. 74–82, 2006, doi: 10.1039/b511524h.

[53] P. Vatankhah and A. Shamloo, “AC SC,” *Anal. Chim. Acta*, 2018, doi: 10.1016/j.aca.2018.03.039.